CDF/ANAL/BOTTOM/CDFR/11173
Version 1.2
August 18, 2015

Measurement of low p_T D^+ meson production cross section at CDF II

Jeffrey A. Appel, Luigi Marchese[1], Manuel Mussini, Luciano Ristori, Diego Tonelli

Abstract

We report a measurement of the of low-p_T D^+-meson production cross section in proton-antiproton collisions at 1.96 TeV center-of-mass energy, using the full data set collected by the CDF experiment at the Tevatron collider during Run II. The measurement is performed in a yet-unexplored $p\bar{p}$ collider low-transverse-momentum range, down to 1.5 GeV/c. The actual QCD theory cannot predict the behavior of the strong interactions in the low transferred-four-momentum region because in these kinematic conditions the strong coupling constant is of the order of the unity. Thus, a perturbative expansion is not useful. At present, several phenomenological models have been proposed, but they are able to describe only a few aspects of the observed physical quantities and not the full complexity. Experimental results in these conditions are then crucial to test new QCD models. The measurement of the differential cross section at low p_T plays an important role in this context, allowing refinement of current knowledge.

Contents

[1]marchese@fnal.gov

1 Introduction

In this note we present the measurement of D^+ meson production cross section in the low-transverse-momentum region. We use fully reconstructed candidates in the $D^+ \to K^-\pi^+\pi^+$ mode and its charge conjugate.

Because of the relatively-large value of the c-quark mass, the production cross section of charm hadrons is several orders of magnitude smaller than that of lighter quarks (u, d and s). A previous published analysis by the CDF Collaboration in 2003 [1] performed this measurement down to a minimum p_T of the D^+ of 6.0 GeV/c, because of the biases introduced by the Two Track Trigger (TTT) selection. Measurements in the region where α_S becomes too big for perturbative calculation and the color confinement behavior is not well understood are crucial. The extension of the previous CDF published measurement for the $D^+ \to K^-\pi^+\pi^+$ cross section at low p_T can give an additional important lever arm to refine the current knowledge and theory. To extend the previous measurement down to a $p_T(D^+)$ as low as 1.5 GeV/c, we use the Minimum Bias (MB) and Zero Bias (ZB) data samples. The ZB and the MB triggers impose minimal and generic requests in order to reduce biases to the physics properties of the collected data, at the price of a reduced fraction of heavy-favor events compared to the large light-quark background. However, in the full 10/fb sample of Run II data, the size of these minimally-biased samples is such that a significant number of charm decays may be present and allow reconstruction of visible exclusive signals.
Theoretically, the cross section for the inclusive production of X_c mesons can be modeled by the convolution of universal parton distribution functions (PDFs) and universal fragmentation functions (FFs) with calculable hard-scattering cross sections via perturbative approach. Early CDF results on D mesons did not agree with theory [2] [3]. Nowadays, the predictions have been improved and calculations with the FONLL(Fixed-Order + Next-to-Leading-Log) [20] expansion are available.
At present, exepriments of the CERN LHC proton-proton collider are the most powerful c-factory in the world. Alice measured the charm production cross-section at low-p_T at a center of mass energy $\sqrt{s} = 7\,TeV$ [5]. However, the present measurement maintains its uniqueness. In fact the different experimental conditions don't reproduce those of Tevatron, both in terms of initial state ($p\bar{p}$) and center of mass energy ($\sqrt{s} = 1.96\,TeV$). Different processes can occur at different energy scales: the comprehension of the energy dependence in non-pQCD is one of the most important questions.

2 Charm physics at CDF

CDF gave one of the most important contribution to the understanding of the production of charmed hadrons in hadron collisions. Before CDF, charm physics had not been done in hadron collisions. The CDF Silicon Vertex Tracker (SVT) was designed to collect large samples of B hadrons in fully hadronic final states,

but thanks to this tracker, CDF was also able to collect huge samples containing D-meson decays, becoming competitive in terms of sensitivity to previous charm factories [6].
On the other side some limitations for charm physics at CDF are due to physics and detector constraints:

- **Limited particle identification.** The Time-Of-Flight detector had π/K separation $\geq 2\sigma$ for $p_T \leq 1.6$ GeV/c, while dE/dx could also help a bit in these conditions. However, CDF had no powerful PID over the full momentum spectrum of interest.

- **Secondary charm.** B hadrons preferentially decay into charm hadrons. Due to the long B lifetime, charm hadrons could be produced at a significant distance from the primary vertex (PV), resulting in a bias to the proper time measurement if the B decay vertex was not reconstructed. The impact parameter distribution of the charm candidate can be very helpful to disentangle direct from secondary charm. In Figure 1 is shown a *prompt* D^+ (directly produced in the $p\bar{p}$ interaction) and a *secondary* D^+ (produced from a B^- decay).

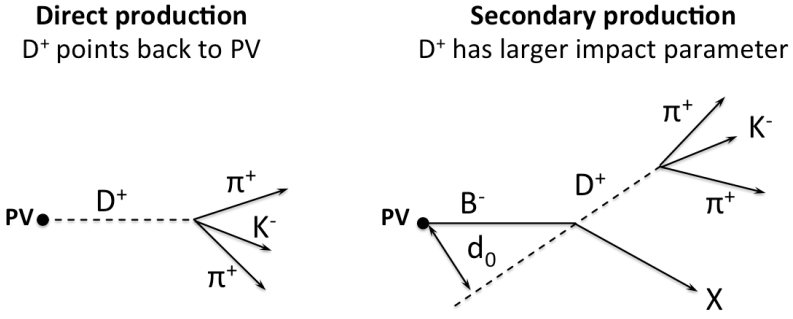

Figure 1: *Sketch of the geometry of final-state particles in primary (left) and secondary (right) charm production, in the transverse plane.*

In this note we present the measurement of the D^+ meson differential production cross section $d\sigma/dp_T$, integrated over y between -1 and +1. and averaged over a number distinct p_T bins.

$$\frac{d\sigma_{D^+\to K^-\pi^+\pi^+}}{dp_T}(p_T; |y| \leq 1) = \left.\frac{\frac{N_{D^+}+N_{D^-}}{2}(p_T)}{\Delta p_T \cdot L \cdot \varepsilon_{trig} \cdot \varepsilon_{rec}(p_T) \cdot \mathcal{B}(D^+ \to K^-\pi^+\pi^+)}\right|_{|y|\leq 1} \quad (1)$$

where:

- N_{D^+} and N_{D^-} are the yields of the D^+ and D^- signals in each bin of p_T. We report the cross section only for D^+ mesons while we measure the yields for both, D^+ and D^- mesons. We include a factor 1/2 because what is actually measured is the average cross section for D^+ and D^- mesons. We postulate charge invariance in the production process through the strong interaction. See Sec. 5.
- Δp_T is the bin width.
- L is the integrated luminosity of the data sample. See Sec. 3.3.
- ε_{trig} is the efficiency associated with the trigger selection. See Sec. 6.1.
- ε_{rec} is the global reconstruction efficiency of our candidates. This parameter takes into account geometrical and kinematical acceptances as well as the detector reconstruction efficiency of the signal. See Sec. 6.2.
- $\mathcal{B}(D^+ \to K^-\pi^+\pi^+)$ is the decay branching ratio of the channel used in this analysis.
- $|y| \leq 1$ is the rapidity range considered: the central region of the detector.

In general the average value of cross section in bin i, $\sigma/\Delta p_{T,i}$, differs from the value corresponding to the p_T value of the center of the bin. We report the differential cross section $d\sigma/dp_T$ integrated over the width of each bin. In order to simulate correctly the data sample, we reweighted the cross section distribution used to generate the simulated signal to match the one observed in data.

We perform a data-driven analysis based on $D^+ \to K^-\pi^+\pi^+$ decays reconstructed in minimally biased sample of data using the central tracker down to $p_T(D^+)$ of 1.5 GeV/c. In each p_T range, we optimize the offline selection using data only, and use mass fits to separate signal from combinatorial backgrounds and simultaneous impact parameters fits to separate charm mesons produced directly in the hard scattering from those resulting from B hadron decays. Reconstruction efficiencies are determined through Monte Carlo simulations after validating its reliability using data.

3 Data Selection

3.1 $D^+ \to K^-\pi^+\pi^+$ at CDF II

The decay channel[2] $D^+ \to K^-\pi^+\pi^+$ offers a convenient final state for straighforward reconstruction of charged D mesons in CDF II; the 9.4% branching fraction guar-

[2]From now, we write in term of D^+, but all the considerations are also true for the D^-.

antees a significant signal yield, and the presence of three charged particles allows exploting the good tracking capabilities of the detector. In addition, there is no ambiguity in the assignment of the masses to the tracks: we know that the two tracks with the same charge are pions. These properties give us a good chance to extract the D^+ meson signal from the background of light particles (mainly pions and kaons) several orders of magnitude larger.

The large average lifetime of the D^+, $\tau = (1040 \pm 7) \cdot 10^{-15}\ s$, corresponds to a $c\tau = 311.8\ \mu m$. The flight distance can be measured thanks to the resolution of the silicon tracker SVX II. In Figure 2 is sketched out the topology of the D^+

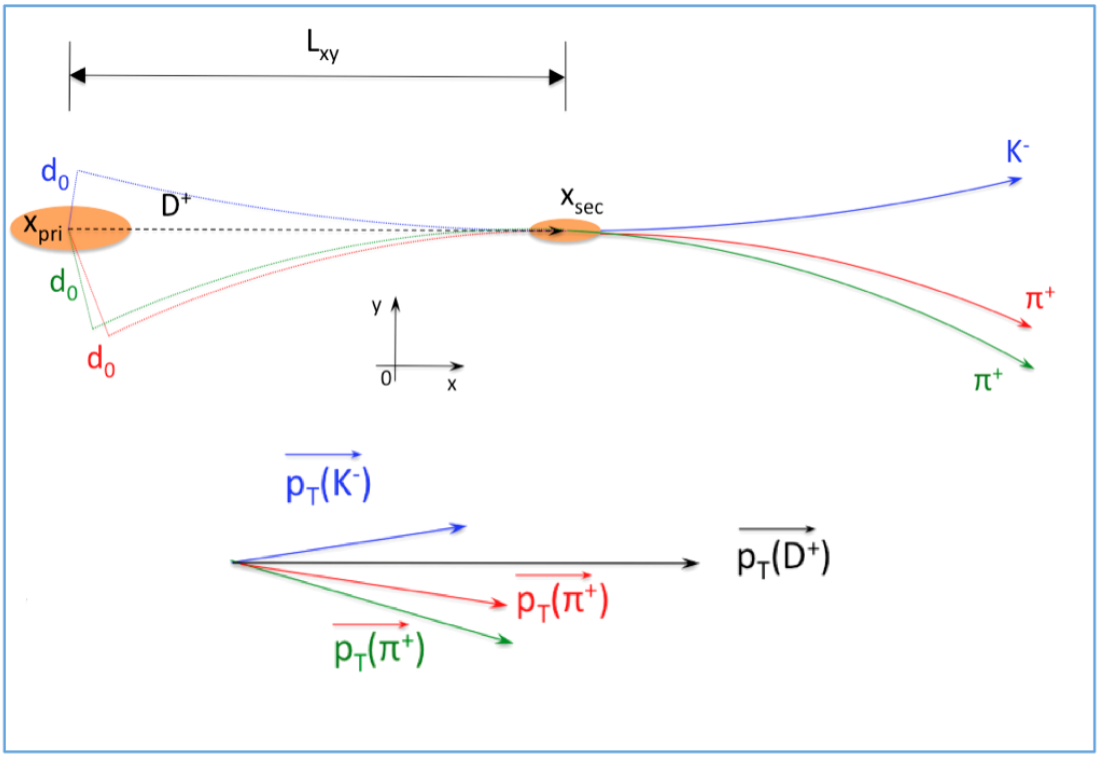

Figure 2: *Graphical representation in the plane of the decay channel* $D^+ \to K^-\pi^+\pi^+$.

decaying to $K^-\pi^+\pi^+$ stressing the relevant variables used in this analysis:

- the **transverse plane** is the plane perpendicular to the proton beam direction $(0xy)$;
- $\vec{x}_{pri}$ - the **primary vertex** - is the point where the $p\bar{p}$ collision takes place. It is located within the beam pipe and it represents the point where the meson is produced: D^+ **origin vertex**;

- $\vec{x}_{sec}$ - the **secondary vertex** - is the decaying point of the D^+;
- $\vec{p}_T$ - the **transverse momentum of the particle** - is the projection of the momentum vector to the transverse plane (writing p_T we refer to its magnitude);
- L_{xy} - the **transverse decay lenght** - is the signed distance in the transverse plane between the primary and the secondary vertices projected to the $\vec{p}_T$ direction. It is defined as follows:

$$L_{xy} = \frac{(\vec{x}_{sec} - \vec{x}_{pri}) \cdot \vec{p}_T}{p_T}; \tag{2}$$

- d_0 - the **impact parameter** - is the signed distance between the origin vertex and the helix of a track at their closest approach to the beamline;
- Δz_0 - the **longitudinal distance** - is the difference between the z coordinate (not shown in Figure 2) of the tracks at their closest approach to the beamline;
- $\Delta\varphi_0$ - the **transverse opening angle** - is the difference between the φ_0 angle (not shown in Figure 2) of the decay tracks at their closest approach to the beamline.

3.2 Online

The published CDF measurement of the D^+ production cross section [1] extends to the minimum $p_T(D^+)$ of 6.0 GeV/c because the data set is selected by a trigger selection with hard requests in terms of transverse momentum of the meson decay products. In our case, in order to reach $p_T(D^+)$ values down to 1.5 GeV/c, we remove any possible bias from the trigger selection. We use the samples collected by the `ZEROBIAS` and the `MINBIAS` trigger paths. The samples have been collected during the whole Run II of the experiment (about 10 years of data taking, from February 2002 to September 2011) and they correspond to a total Tevatron delivered luminosity $L_{dev} = 10/\text{fb}$.

3.2.1 The Zero Bias trigger

The first trigger used in this analysis is the `ZB`. It does not bases its decision on any information associated to the detector; it just samples randomly $p\bar{p}$ bunch crossings independently of whether the crossing produced a hard $p\bar{p}$ scattering or not. In order not to overcome the maximum output rate to the disk, the event rate must be reduced by a prescale factor; this happens only at L1. The ZB requirements to trigger an event are the followings:

Level 1: any bunch crossing fires L1. Prescale factor = 1,000,003.

Level 2: no restrictions, any event is automatically accepted by L2.

Level 3: no requests.

About 177 millions of events are collected by this trigger.

3.2.2 The Minimum Bias trigger

The second trigger used for this analysis is the `MB`. The aim of this trigger is to identify and select only crossings resulting in, at least, an inelastic $p\bar{p}$ collision. The main restrictions apply at L1 exploiting the CLC subdetectors. L1 fires when at least one East CLC signal is in coincidence with a signal in at least one West CLC. Considering the typical Tevatron initial luminosity, almost all the bunch crossings result in a hard collision. As a consequence, the MB output rate would be higher than the maximum output rate to disk. A prescale factor is applied: one event is triggered by L1 every 100,003 times this coincidence occurs. For the same reason further rate limitations occur at L2 and L3 reducing the trigger rate to one event per second. The MB requirements to trigger an event are the followings:

Level 1: CLC signals coincidence. Prescale factor = 100,003.

Level 2: any event is automatically accepted by L2. Rate limit = 3 Hz.

Level 3: any event is automatically accepted by L3. Rate limit = 1 Hz.

About 123 millions of events are collected by this path.

3.2.3 Samples overlap

During the data acquisition, the ZB and MB trigger selections operate at the same time. Events might be collected by both triggers and appear twice in the sample. Without prescales, all the times a collision happens and the crossing is triggered by the CLCs coincidence, also the ZB trigger is fired. On the contrary, bunch crossings with no interaction won't be triggered by the CLC coincidence. Thus the `MINBIAS` sample would in principle be a subset of the `ZEROBIAS` sample. Because of the prescale factor and the rate limits imposed to the `MINBIAS` trigger path, a reduction factor of $\sim 10^6$ is imposed on the overlapping events. Only 194 events are present in both samples. We use them only once, getting a negligible impact on the estimated integrated luminosity with respect to its uncertainty.

3.3 Good Run List and luminosity

We use the official QCD good run list (GRL) that contains only runs where SVX II and the COT were working properly. The small fraction of runs for which the database reports unreliable luminosity values are discarded. After these requests the ZB sample isreduced to ~ 183 million events while the MB sample to ~ 133 million events.
Thanks to the measured rate of the inelastic $p\bar{p}$ events, $R_{p\bar{p}}$, it is possible to estimate CDF II instantaneous luminosity by the following equation:

$$\mathcal{L} = \frac{R_{p\bar{p}}}{\sigma_{in} \cdot \epsilon_{CLC}} \tag{3}$$

where σ_{in} is the inelastic $p\bar{p}$ cross section at $\sqrt{s}$ = 1.96 TeV and ϵ_{CLC} is the CLCs acceptance. The only direct measurement of σ_{in} at the Tevatron has been performed at the beginning of Run I. At that time the center of mass energy was 1.8 TeV [7]. Unfortunately, the inelastic cross section has not been measured anymore, even when the Tevatron achieved the higher and last center of mass energy of $\sqrt{s}$ = 1.96 TeV. The instantaneous luminosity used in the online and offline calculations is obtained by extrapolating the CDF and E811 combined measurements at $\sqrt{s}$ = 1.8 TeV to the project expected value $\sqrt{s}$ = 2 TeV. Even if the value of 2 TeV was never reached, for historical reasons the expected value has been used, overestimating the total $p\bar{p}$ cross section by about the 1.9%. The raw integrated luminosity stored on the database is corrected for the 1.9% factors, as listed in Table 1 to derive the actual trigger luminosity of the sample
L_{Trig} $(= L_{Raw} \cdot 1.019)$.

	L_{Raw}	$L_{Raw} \cdot 1.019$
ZB	8.90	9.07
MB	6.83	6.96
Tot	15.73	16.03

Table 1: *Luminosity corrections for ZB, MB and total samples in* $(nb)^{-1}$.

In [8] the systematic uncertainty on the measured luminosity is assessed to be ~ 6%.

3.4 Candidate selection

In each event, the D^+ candidates are reconstructed offline by combining all the possible triplets of tracks into a kinematic fit. We select tracks only in the η and p_T ranges where the reconstruction of the tracking system is efficient.

The base quality requirements for each track are as follows:

- SVX II small angle stereo hits ≥ 1;
- SVX II stereo hits ≥ 2;
- SVX II axial hits ≥ 3;
- COT stereo hits ≥ 25;
- COT axial hits ≥ 25;
- $|\eta| \leq 1.2$;
- $p_T \geq 0.4$ GeV/c;
- $0 \leq |d_0| \leq 1$ mm.

The hit requirements follow the standard prescriptions in heavy flavor analyses. We also introduce fiducial requirements that ensure that each track is reconstructed in the portion of tracking volume where COT and SVX detectors have optimal performances [9]:

- $|z| \leq 155$ cm at radius R = 133 cm;
- $|z| \leq 47.25$ cm at radius R = 10.645 cm.

We consider all the possible triplets of tracks which pass the above selection. A triplet of good tracks is expected to satisfy the following criteria:

- $|\sum_{i=1}^{3} q_i| = 1$;
- $d_{0,max} \cdot d_{0,min} < 0$;
- $\Delta\varphi_{0,min} = |\varphi_{0,i} - \varphi_{0,j}| \geq 2°$;
- $\Delta z_{0,max} = |z_{0,max} - z_{0,min}| \leq 3$ cm;

where the index `i` and `j` refer to the tracks of the triplet; q_i is the charge of the track `i`; $d_{0,max}$, $d_{0,min}$, $z_{0,max}$, $z_{0,min}$ represent the maximum or the minimum value of the impact parameter d_0 or of the z_0 coordinate of the three tracks; $\Delta z_{0,max}$ and $\Delta\varphi_{0,min}$ represent the maximum and minimum variation of the z_0 coordinate and φ_0 among the tracks of the triplet. We ask for $\Delta\varphi_{0,min} \geq 2°$ to avoid ghost tracks: during the event reconstruction, for redundancy reasons, different pattern recognition alghoritms work indipendently, so the same track could be reconstructed by two of them with slightly different parameters and counted twice.

We fit the three tracks looking for a possible common origin point displaced from the primary vertex. We define the z coordinate of the *origin* vertex as the

weighted average of the tracks z_0. At this z coordinate we evaluate the beam position in the transverse plane and we set the x and y coordinates of the origin of the candidate. The fit converges only if the helices are within a certain threshold in the longitudinal direction. The track steering method is implemented: every time the fit is perfomed again using the primary vertex as an additional point for each of the three tracks. A successful fit returns the candidate's decay vertex, the resulting global χ^2 of the fit and the new re-fitted tracks. We have a candidate if the result of the fit satisfies the following base requests:

- $L_{xy} \geq 0$ cm;
- $|y(D^+)| \leq 1$;
- $\chi^2_{red} \leq 10$;

where $y(D^+)$ is the candidate's rapidity and χ^2_{red} is the χ^2 of the fit divided by the number of degrees of freedom (n.d.f.).

In Figure 3 we show the invariant $K^-\pi^+\pi^+$ mass distribution of the candidates, selected as described above. No signal is observed with the base selection alone. A selection optimization is required.

3.5 Selection optimization

One of the main challenges of the present work is the optimization of the candidate selection in order to reduce the light-meson background, intially 10^4 times larger than the signal, as described in [10].
A pure data-driven optimization is introduced in a way that leads to unbiased sample selection. The optimization strategy of the selection is performed *independently* in each $p_T(D^+)$ bin. The statistics available is enough to probe the $p_T(D^+)$ range [1.5; 14.5] GeV/c in bins of variable size.

Let $\mathcal{M}$ be the data sample on which the selection is optimized.

1. The event number is used as a random criterion to divide the sample $\mathcal{M}$ into two statistically independent subsamples with approximately the same size, even-numbered and odd-numbered events.

2. A configuration space is built considering three optimization variables. After studying several variables, we individuate the three able to select the maximum number of signal events over background events: $p_T(TRK^3)$, the transverse momenta of the decay tracks, the χ^2 returned by the kinematic fit

[3] From now, we write TRK meaning one of the decay TRacKs.

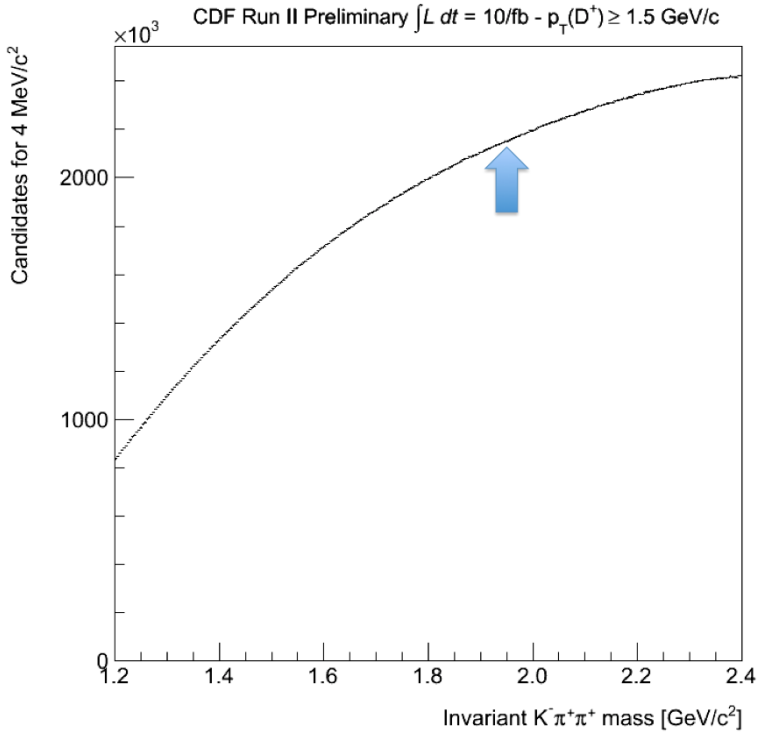

Figure 3: *Invariant $K^-\pi^+\pi^+$ mass distribution of the candidates obtained using the selection described in Sec. 3.4. The arrow indicates where the D^+ peak is expected.*

of the decay, and L_{xy}. We consider ten possible steps, different values of the cut, applied to each variable. The *i-th* element of the configuration space is a possible different combination of the cuts applied to the three variables:

- Two $p_T(TRK) \geq p_{T,j}$;
- $\chi^2_{red} \leq \chi^2_{red,m}$;
- $L_{xy} \geq L_{xy,n}$.

Variable	Range	Step
Two $p_T(TRK)$	[0.4; 1.3] GeV/c	$p_{T,j}$ [0.1 GeV/c]
χ^2_{red}	[10; 0]	$\chi^2_{red,m}$ [1]
L_{xy}	$[0; 1450]\mu m$	$L_{xy,n}$ [150 μm]

Table 2: *Variables used for the optimization procedure.*

3. Considering the *i-th* configuration, signal ($\mathcal{S}_i$) and background ($\mathcal{B}_i$) are obtained through a binned likelihood fit on the invariant $K^-\pi^+\pi^+$ mass plot,

within 2σ around the D^+ peak (*Signal Region*). The figure of merit is defined as:

$$f(\mathcal{S}_i, \mathcal{B}_i) = \mathcal{S}_i/\sqrt{\mathcal{S}_i + \mathcal{B}_i}. \quad (4)$$

It is used to minimize the statistical uncertainty on the measured signal.

4. Considering the even subsample E, the configuration space is scanned in order to find the parameters that maximize our figure of merit, $f(\mathcal{S}^E, \mathcal{B}^E)$. The selection corresponding to the maximum of f optimizes $f(\mathcal{S}^E, \mathcal{B}^E)$.

5. The last two steps are repeated using the odd sample O to obtain the set of cuts which optimize the sample O. Due to statistical fluctuations, they are in general different from the ones obtained in sample E.

6. The final sample is obtained applying to the subsample E the requirements optimized in subsample O and viceversa.

Splitting the sample $\mathcal{M}$ as described avoids a bias in the selection and, at the same time, uses all the available statistics.
Figure 4 graphically describes the complete procedure.

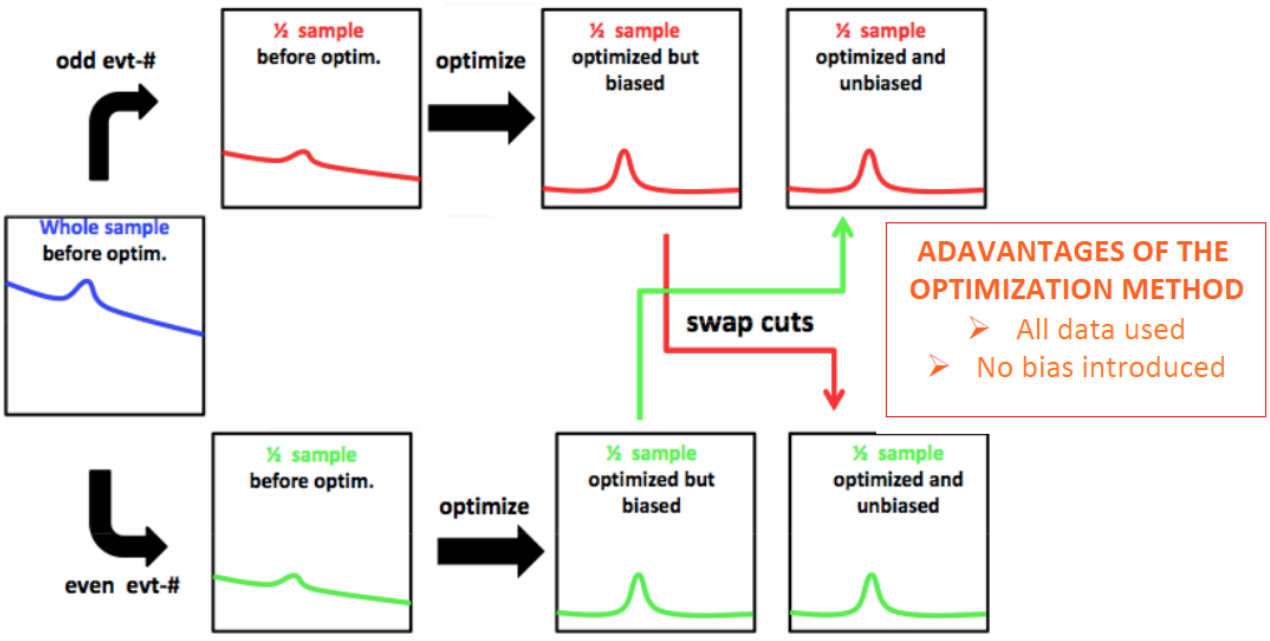

Figure 4: *Graphical scheme of the complete optimization strategy [11].*

In Table 3 we show the optimized cuts in different bins of $p_T(D^+)$ for the even and odd subsamples.

$p_T(D^+)[GeV/c]$	Subsample	$p_{T,j}$ [GeV/c]	χ^2_m	$L_{xy,n}$ $[\mu m]$
[1.5; 2.5]	Even	0.7	4	600
	Odd	0.6	4	600
[2.5; 3.5]	Even	0.6	2	600
	Odd	0.6	3	600
[3.5; 4.5]	Even	0.7	5	750
	Odd	0.7	6	750
[4.5; 6.5]	Even	0.9	6	750
	Odd	0.9	6	750
[6.5; 14.5]	Even	1.1	7	750
	Odd	1.1	7	750

Table 3: *Optimized cuts in different bins of* $p_T(D^+)$ *for the even and odd subsamples.*

4 Monte Carlo (MC) samples

We use MC samples in this analysis for different purposes:

- derive mass and impact-parameter templates for the yields fits for each bin of p_T. Such shapes are needed to perform the fit of the yields (See Sec. 5);
- derive impact-parameter distributions of D^+ mesons from b hadron decays used to separate the prompt fraction (See Sec. 5.1);
- estimate the reconstruction efficiency of our selection (See Sec. 6.2).

The BGENERATOR is used in the CDF B MC. This generator is explicity designed for beauty and charm physics. It simulates the production and fragmentation of b and c quarks and the resulting hadrons are decayed using QQ (the CLEO Monte Carlo generator adapted for CDF II package).
The BGENERATOR algorithm needs the joint distribution of transverse momentum and rapidity for the generated quark as input information. We use realistic input distributions that scan the $y - p_T$ plane in $[-1.3,\ 1.3] \times [0,\ 15]$ GeV/c. In order to reproduce the same online selection, no trigger simulation and selection is performed. Also, to have a more detailed simulation of the actual experimental conditions, the off-line database is used to tune the simulation. In such a way, on

a run by run basis, many of the major variations in configuration are taken into account. So, a detailed simulation of real runs is available, allowing to match, in any given sample, the distribution of data and MC. To analyse simulated data with the same reconstruction programs used for data, the two samples share the same output format. The MC events follow the same reconstruction chain as data and, after the detector simulation, we apply the same candidate selection performed on data. The MC events are distributed across the data-taking periods $P0 - P38$, in proportions that approximate the integrated luminosity collected in each period.

4.0.1 $D^+ \to K^-\pi^+\pi^+$

We generate a sample of about 75 million D^+ and D^- mesons in equal proportion, forced to decay into the $K^-\pi^+\pi^+$ final state. This sample is used to derive mass and impact-parameter templates to be used in the yield fits. In Figure 5 the resulting invariant $K^-\pi^+\pi^+$ mass distribution in linear and logarithmic scale is shown. The plot shows a narrow peak centered at the known D^+ mass with a width of about 7 MeV/c^2. A long tail at lower masses is evident: it represents the soft-photon emission.

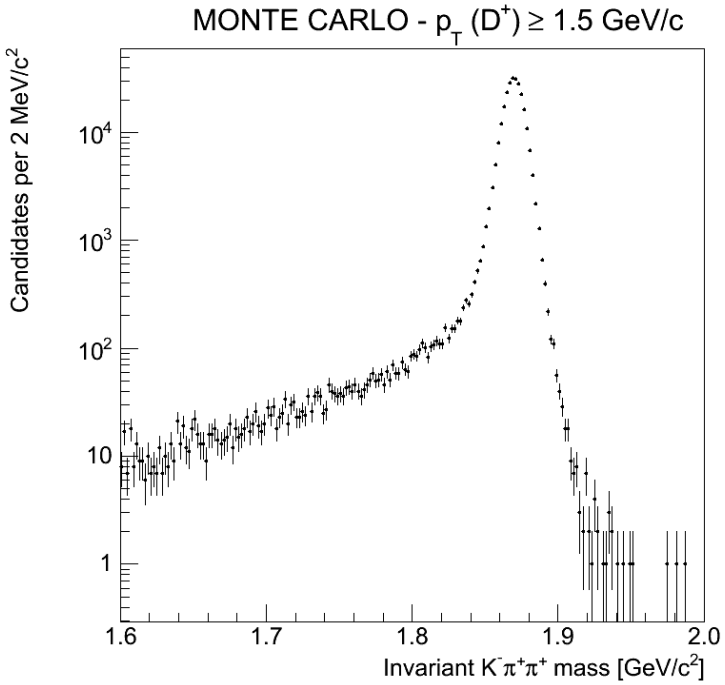

Figure 5: *Invariant $K^-\pi^+\pi^+$ mass distribution of candidates reconstructed in the $D^+ \to K^-\pi^+\pi^+$ MC sample.*

4.0.2 $B^{\pm/0} \to D^+ X$

We generated a sample of 36 million B^0 and 36 million $B^\pm$ decays forcing them to decay only into channels involving at least one D^+ in the final state. We forced the charm mesons to decay into $K^-\pi^+\pi^+$ final states. This sample is used to define the templates which describe the secondary D^+ sample coming from B decays.

4.0.3 $D^+ \to K^-\pi^+\pi^+$ with underlying events

From a previous study [17] we know that the signal-only MC does not correctly reproduce the COT occupancy and thus the number of hits associated with each track; it results in a wrong simulation of the single track *absolute* reconstruction efficiency of the COT. We then generated our sample with additional MB interactions as underlying events of our D^+ signal as suggested in [17]. The primary vertices distribution of this simulation doesn't match perfectly the real primary vertices distribution in each data-taking period. We reweight the MC primary vertices distribution to mimic the real primary vertices distribution. We divide out data into five different time periods along the 10-year duration of Run II. Figures 6 and 7 show the MC primary vertices distributions for each data-taking period before that we reweight.

This sample is used to measure the D^+ reconstruction efficiency, as we will explain in Sec. 6.2.

5 Yields as a function of $p_T(D^+)$

In order to find the D^+ yield, a two-dimensional unbinned likelihood fit to the invariant $K^-\pi^+\pi^+$ mass and to the candidate-impact parameter distribution is performed.
It is assumed that in the signal region there are only three components: prompt, secondary and combinatoric. As described in Sec. 2, the D^+ produced directly at the point where the primary $p\bar{p}$-interaction occured is the signal we are measuring, the prompt component. Some D^+ can originate from decays of B mesons. They constitute a secondary component which is caracterized by a wider impact parameter distribution than the prompt component. Three unrelated tracks with an effective mass near the D^+ peak value in the invariant mass distribution form a combinatoric backgorund.
Using only the information from the invariant mass distribution, it is not possible to distinguish between primary and secondary D^+. The impact-parameter distribution can be used to separate the two components. The shapes for the prompt and secondary impact-parameter distributions are determined using the Monte

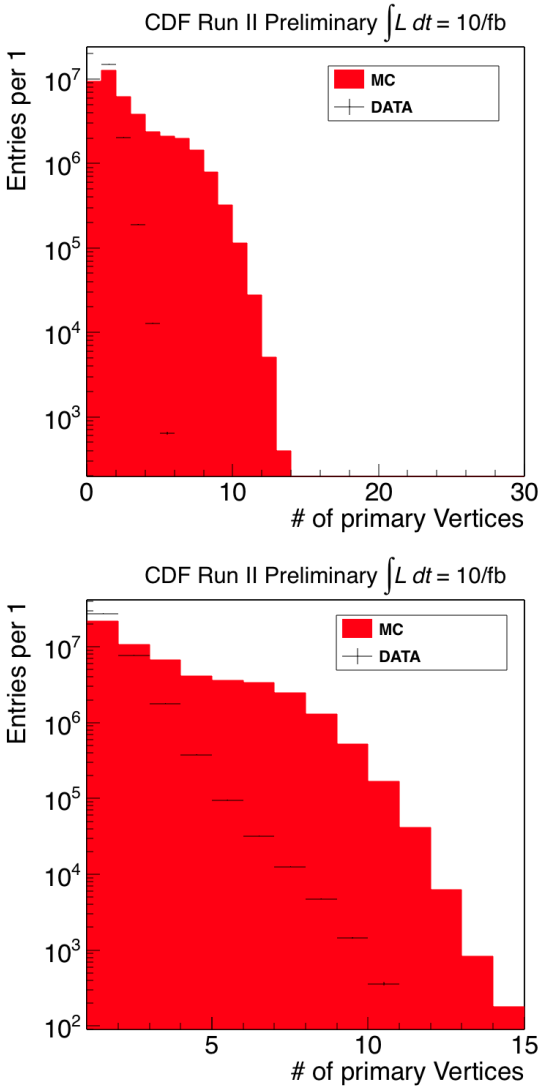

Figure 6: *MC primary vertices distribution (red area) and data (black markers) for the first and second data-taking periods.*

Carlo simulations, while the combinatoric-background shape is determined using data.
For each component, the distributions in mass and impact parameter are uncorrelated. Thus the likelihood function to be maximized is the following:

$$\mathcal{L}(f_P, f_S) = f_P \cdot F_{SP}(m) \cdot F_P(d_0) + f_S \cdot F_{SP}(m) \cdot F_S(d_0) + (1 - f_P - f_S) \cdot F_C(m) \cdot F_C(d_0) \quad (5)$$

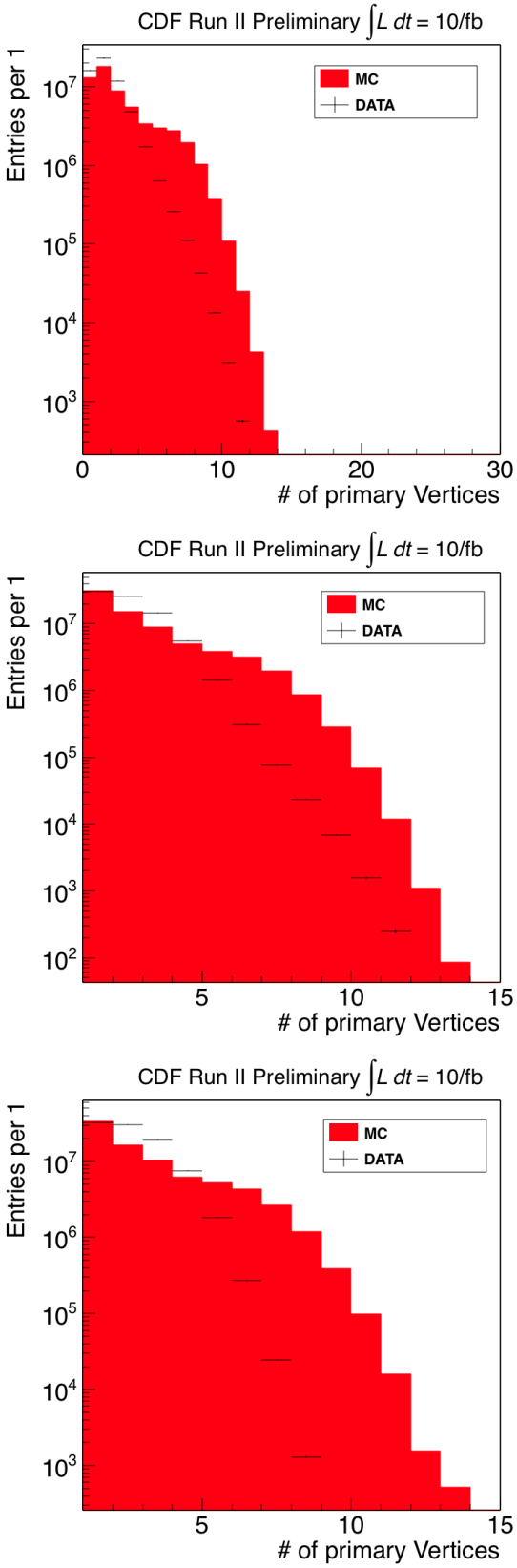

Figure 7: *MC primary vertices distribution (red area) and data (black markers) for the third, fouth and fifth data-taking period.*

where $F_{SP}(m)$ is the common shape in the invariant $K^-\pi^+\pi^+$ mass distribution for the primary and secondary components; $F_P(d_0)$, $F_S(d_0)$ and $F_C(d_0)$ are the shapes in the D^+-impact parameter distribution for the primary, secondary, and combinatoric components, respectively. $F_C(m)$ is the shape in the invariant-mass distribution for the combinatoric component. The free parameters are only the prompt and secondary fractions, f_P and f_S.

The results for the two-dimensional unbinned likelihood fit for the $p_T(D^+)$ bins are shown from Figure 8 to Figure 12. All the results are also summarized in Table 13.

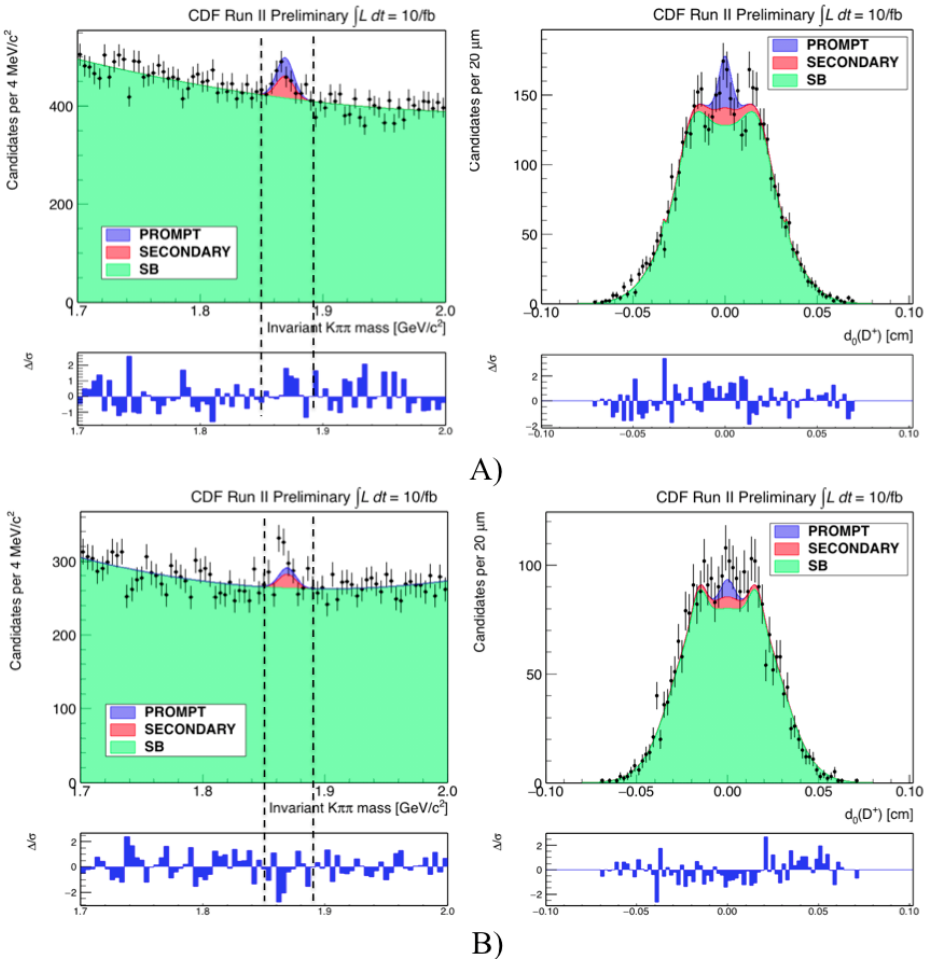

Figure 8: *Two-dimensional unbinned likelihood fit for $p_T(D^+)$ in the range [1.5; 2.5] GeV/c for the even subsample A) and odd subsample B). On the left the results of the fit to the invariant mass distribution are shown, on the right the projection on the impact-parameter axis of the fit function in the signal region.*

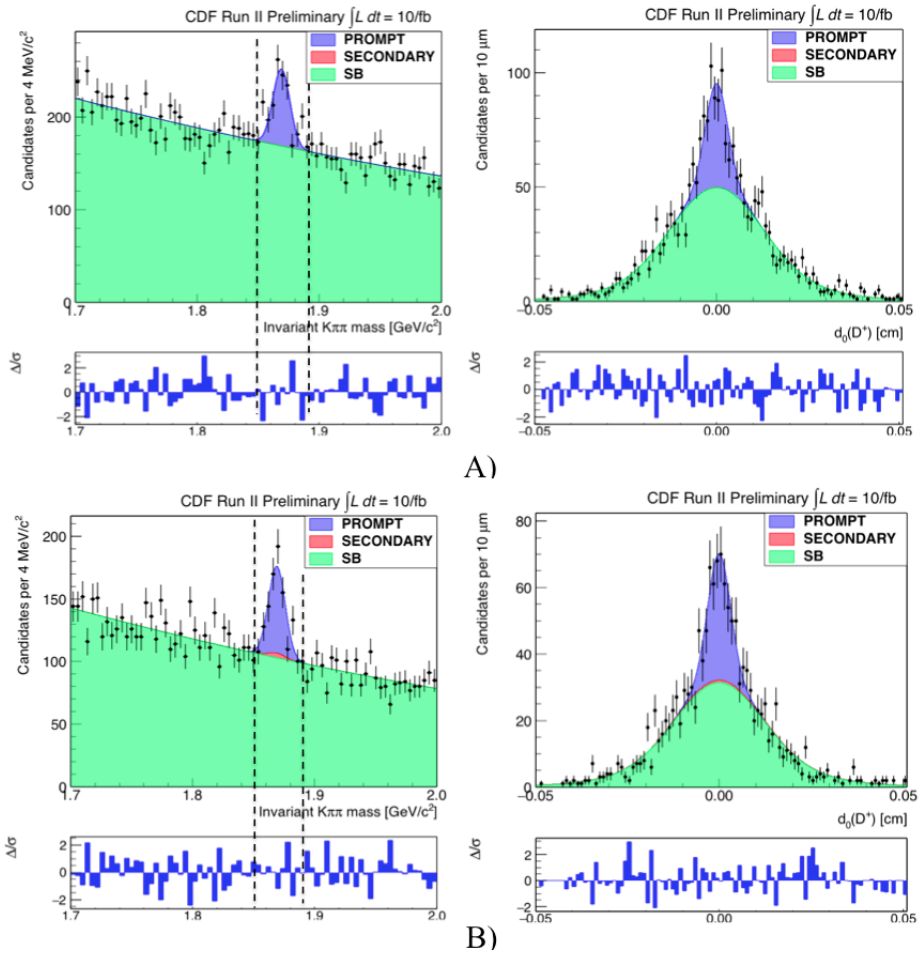

Figure 9: *Two-dimensional unbinned likelihood fit for $p_T(D^+)$ in the range [2.5; 3.5] GeV/c for the even subsample A) and odd subsample B). On the left the results of the fit to the invariant mass distribution are shown, on the right the projection on the impact-parameter axis of the fit function in the signal region.*

5.1 Signal and background shapes

To determine the impact-parameter shapes for the prompt and secondary candidates we use the BMC sample described in Sec. 4.0.1 and 4.0.2 respectively. For each $p_T(D^+)$ bin we parametrize the impact-parameter line shape of prompt and secondary candidates with a sum of three Gaussians. The probability density functions (PDFs) are defined as follows:

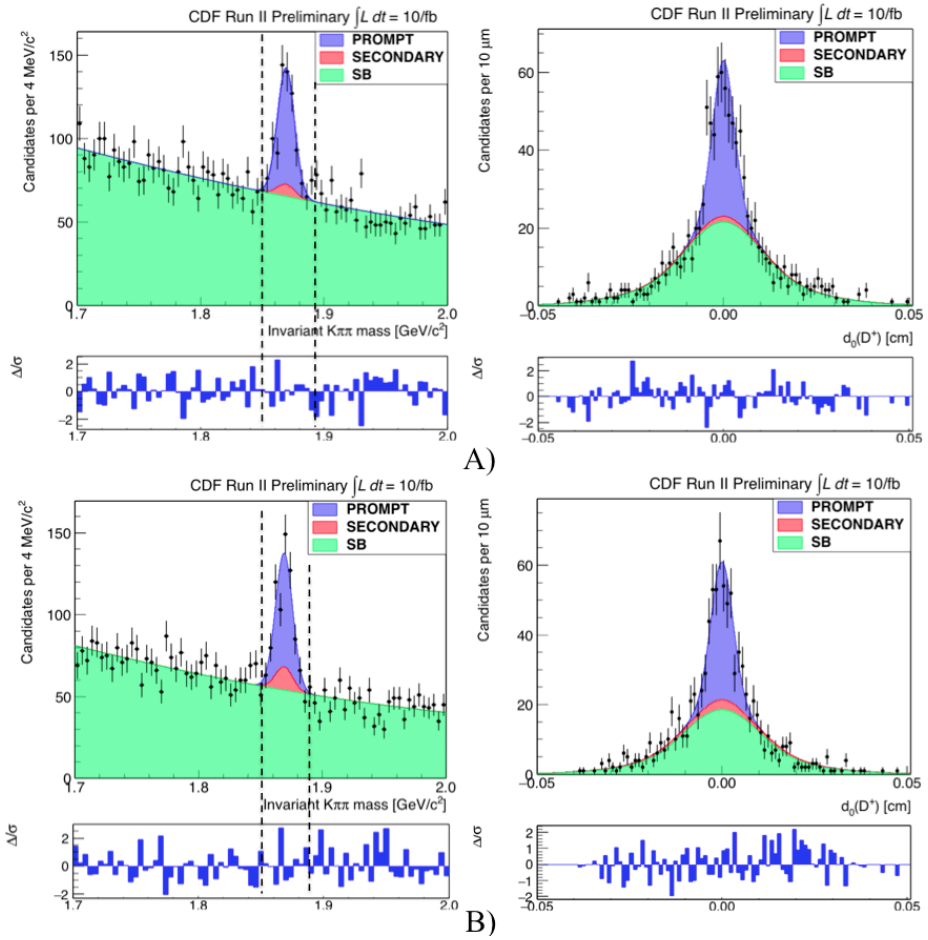

Figure 10: *Two-dimensional unbinned likelihood fit for $p_T(D^+)$ in the range [3.5; 4.5] GeV/c for the even subsample A) and odd subsample B). On the left the results of the fit to the invariant mass distribution are shown, on the right the projection on the impact-parameter axis of the fit function in the signal region.*

$$F_P(d_0;\vec{\theta}_P) = f_{P1}\cdot\mathcal{G}(d_0;\mu_{P1},\sigma_{P1})+f_{P2}\cdot\mathcal{G}(d_0;\mu_{P2},\sigma_{P2})+(1-f_{P1}-f_{P2})\cdot\mathcal{G}(d_0;\mu_{P3},\sigma_{P3}) \tag{6}$$

$$F_S(d_0;\vec{\theta}_S) = f_{S1}\cdot\mathcal{G}(d_0;\mu_{S1},\sigma_{S1})+f_{S2}\cdot\mathcal{G}(d_0;\mu_{S2},\sigma_{S2})+(1-f_{S1}-f_{S2})\cdot\mathcal{G}(d_0;\mu_{S3},\sigma_{S3}) \tag{7}$$

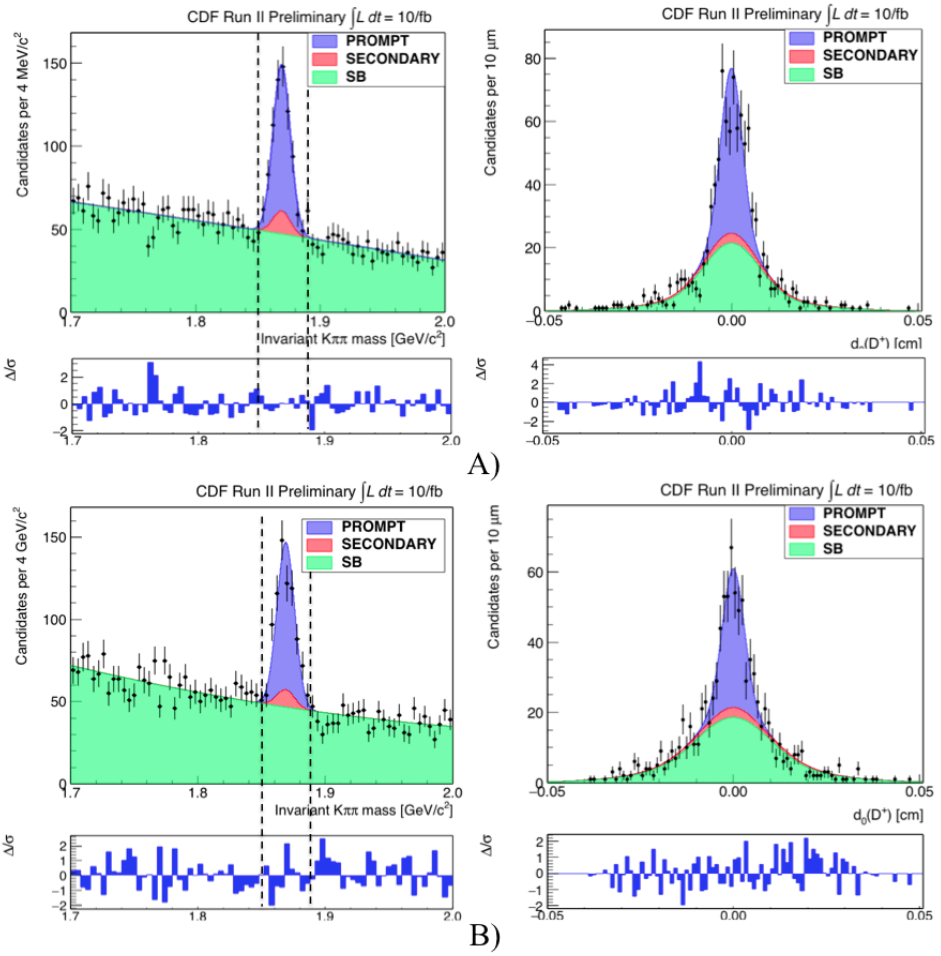

Figure 11: *Two-dimensional unbinned likelihood fit for $p_T(D^+)$ in the range [4.5; 6.5] GeV/c for the even subsample A) and odd subsample B). On the left the results of the fit to the invariant mass distribution are shown, on the right the projection on the impact-parameter axis of the fit function in the signal region.*

From the invariant-mass distribution, we define the side-band (SB) regions as $[1.7; 1.8]$ GeV/c^2 and $[1.9; 2.0]$ GeV/c^2. The combinatoric-background shape comes from the impact-parameter distribution in the side-band regions of the D^+ invariant mass plot. We parametrize the impact-parameter line shape of the combinatoric component with a sum of two Gaussians. The probability density function (PDF) is defined as follows:

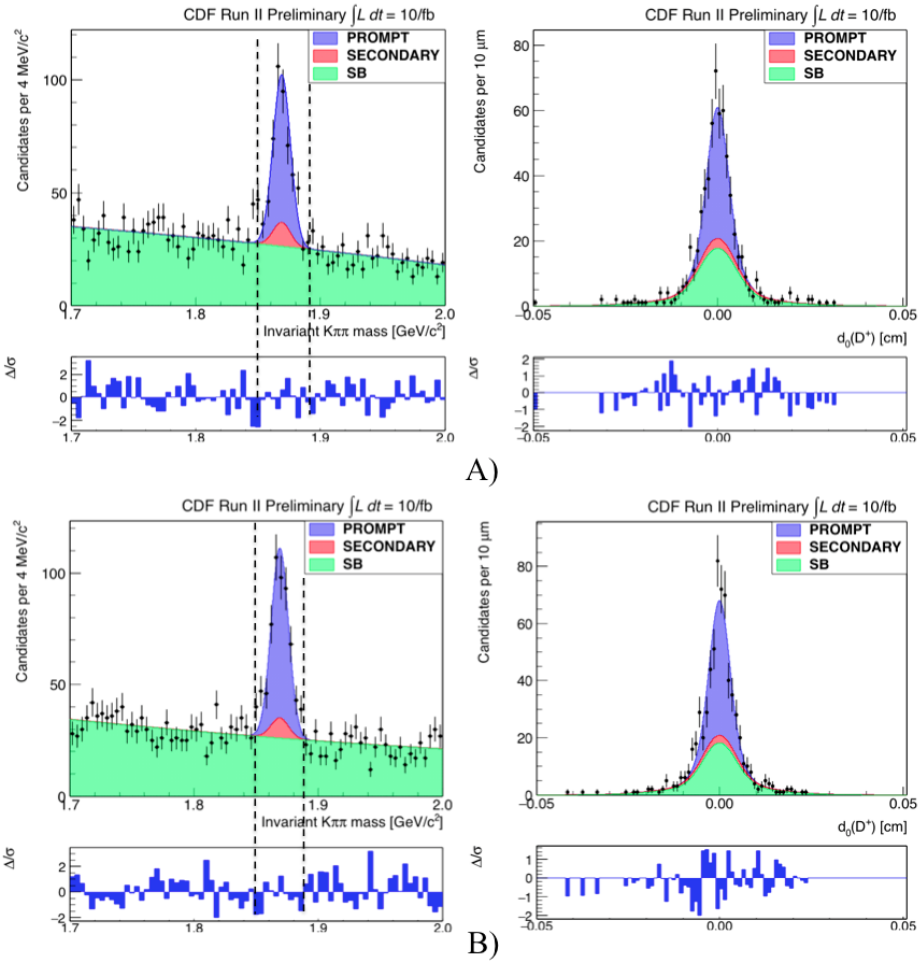

Figure 12: *Two-dimensional unbinned likelihood fit for $p_T(D^+)$ in the range [6.5; 14.5] GeV/c for the even subsample A) and odd subsample B). On the left the results of the fit to the invariant mass distribution are shown, on the right the projection on the impact-parameter axis of the fit function in the signal region.*

$$F_C(d_0;\vec{\theta}_C) = f_{C1}\cdot\ \mathcal{G}(d_0;\mu_{C1},\sigma_{C1}) + (1-f_{C1})\cdot\ \mathcal{G}(d_0;\mu_{C2},\sigma_{C2}) \tag{8}$$

The D^+ mass shapes are modeled from a single fit to the invariant $K^-\pi^+\pi^+$ mass distribution. As explained, the invariant $K^-\pi^+\pi^+$ mass plot is made from two components: prompt and secondary signal together and combinatoric background. We parametrize the line shape with a sum of a Gaussian and a second-order polynomial. The probability density function (PDF) is defined as follows:

$$F_{SP}(m;\vec{\theta}_{SP}) = \mathcal{G}(d_0;\mu_{SP},\sigma_{SP}) \tag{9}$$

$$F_C(m;\vec{\theta}_{Cm}) = Pol2(m;a,b,c) \tag{10}$$

The lowest bin, $p_T(D^+)\ \epsilon\ [1.5;\ 2.5]$ GeV/c, has required a special parametrization. In fact, the combinatorial background shows two structures in the impact-parameter distribution. The impact-parameter pdf is the sum of six Gaussians for this bin:

$$F_C(d_0;\vec{\theta}_C) = f_1\cdot[f_{C1}\cdot\mathcal{G}_1+f_{C2}\cdot\mathcal{G}_2+(1-f_{C1}-f_{C2})\cdot\mathcal{G}_3]+(1-f_1)\cdot[f_{C3}\cdot\mathcal{G}_4+f_{C4}\cdot\mathcal{G}_5+(1-f_{C2}-f_{C3})\cdot\mathcal{G}_6] \tag{11}$$

This effect is due to the selection cuts implemented in this bin, as a result of the optimization procedure. It is evident an high acceptance of poorly reconstructed events in the low p_T region. In fact, it is not reproduced in the MC for the prompt and secondary component, as evident in Figure 13. In Figure 14 we show the signal region before to apply the SBs subtraction and after for $p_T(D^+)\ \epsilon\ [1.5;\ 2.5]$ GeV/c. The SBs-subtracted distribution doesn't show the two structures.

Figures 15 and 16 show the shape parametrization for each component for $p_T(D^+)\ \epsilon\ [3.5; 4.5]$ GeV/c.

6 Efficiencies

The D^+ global efficiency, $\varepsilon(D^+)$, can be defined as the probability a D+ has to pass the trigger, the reconstruction and the offline selection criteria. We restrict the estimation of $\varepsilon(D^+)$ to D mesons reconstructed in the region $|y(D^+| \leq 1$. It is convenient to factorize the efficiency into two main contributions: trigger, ε_{trig}, and reconstruction, ε_{rec}:

$$\varepsilon(D^+) = \varepsilon_{trig}\ \cdot\ \varepsilon_{rec}(p_T)\Big|_{|y|\leq 1} \tag{12}$$

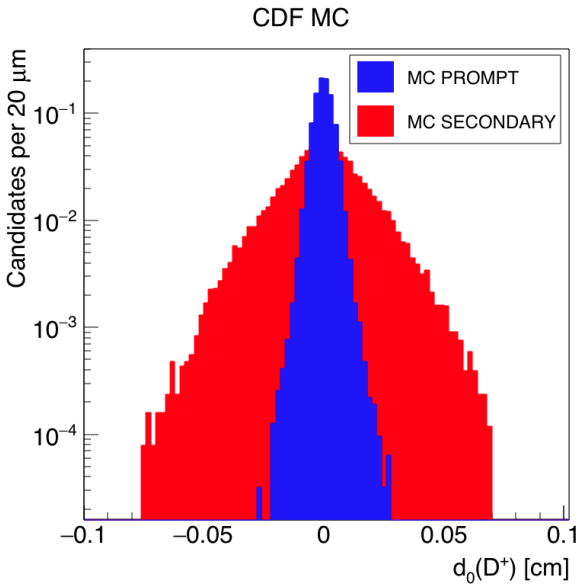

Figure 13: *MC simulation for the prompt and secondary component in the impact-parameter distribution for $p_T(D^+)$ in the range [1.5; 2.5] GeV/c.*

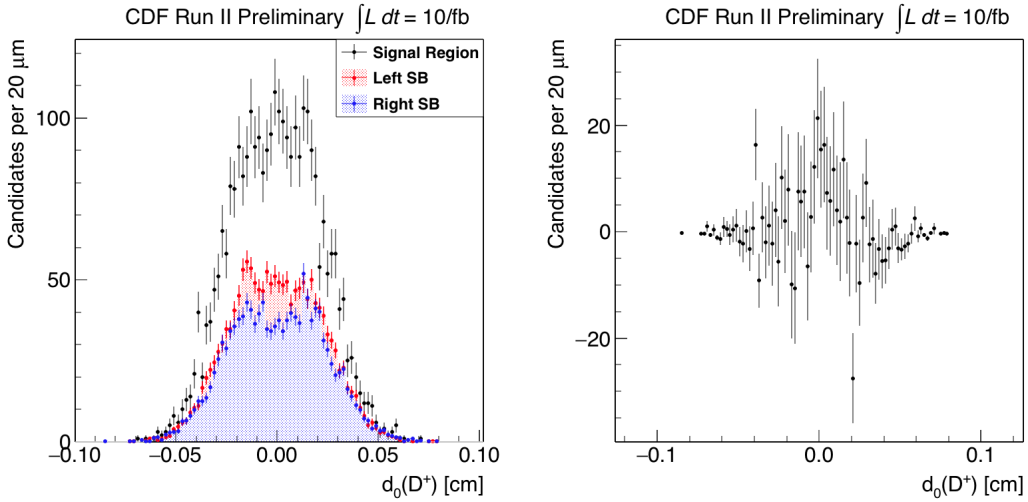

Figure 14: *Impact-parameter distribution for the signal region before to apply the SBs subtraction (left) and after (right) for $p_T(D^+)$ in the range [1.5; 2.5] GeV/c.*

6.1 Trigger efficiency

The term ε_{trig} represents the correction for any inefficiency due to the online data acquisition process and the trigger selection. Each trigger has its own efficiency: ε_{ZB} and ε_{MB}.

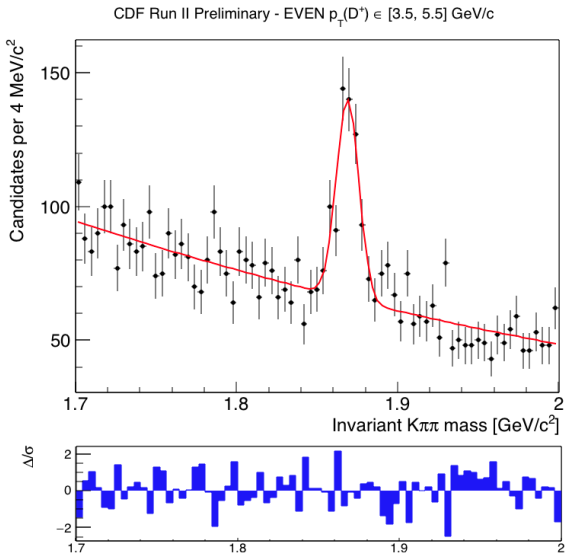

Figure 15: *Shape parametrization for the signal and combinatorial background component in the invariant mass distribution for $p_T(D^+)$ in the range [3.5; 4.5] GeV/c.*

6.1.1 ε_{ZB}

The only possible source of inefficiency for the ZB trigger is the dead time incurred through the three-level trigger chain. However, each trigger path's luminosity is automatically corrected by this non-operating time. Hence, the value stored in the luminosity database does not need to be corrected because of data collection inefficiency and the value for the ZB trigger ε_{ZB} is 1 [13].

6.1.2 ε_{MB}

The MB trigger efficiency may depend on crossing and event conditions as a function of instantaneous luminosity (L_{inst}), number of charged particles in the event, maximum track p_T, overall E_T, pile-up, etc. This is reflected in an increasing efficiency as a function of these variables because the probability of a matching signal in both East and West CLC increases. Several studies to understand these dependencies were performed during Run II [14–16]. Because the ZB trigger path is 100 % efficient, we use data to evaluate the efficiency correction for the MB sample. In fact, each CDF event reports the status for each trigger present in the trigger table. Thus we check if a particular ZB event was also triggered by the `MINBIAS` trigger at L1 and perform a combined fit of the invariant $K^-\pi^+\pi^+$ mass distribution of candidates from events that are selected by the ZB trigger and

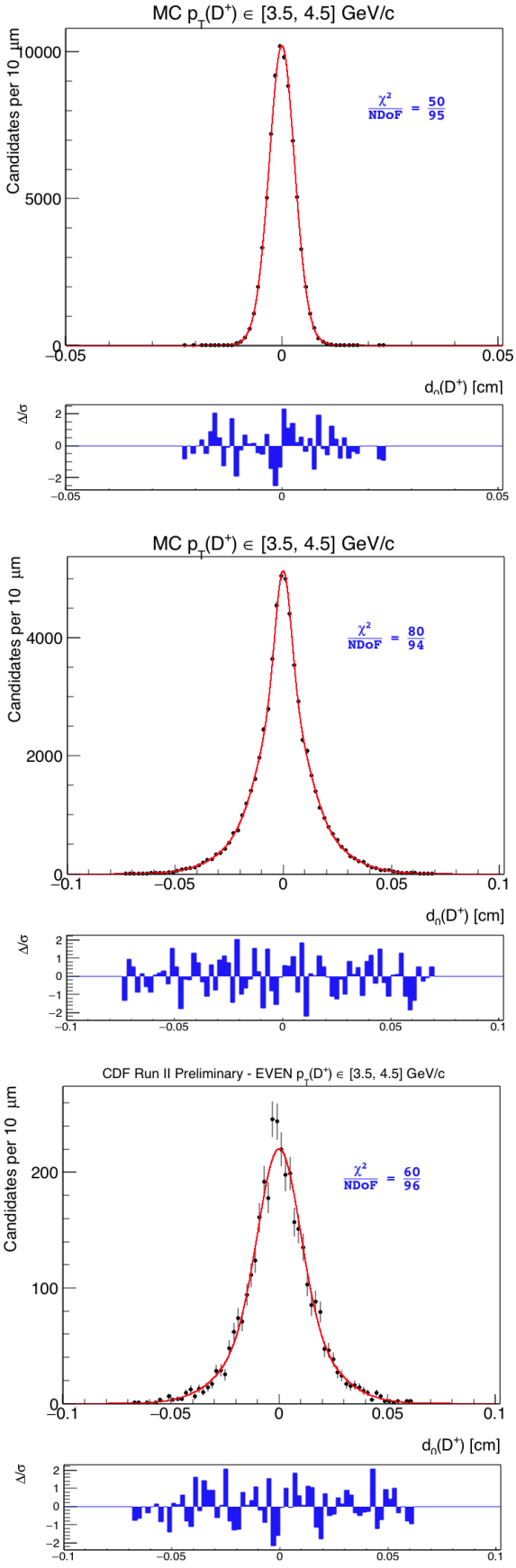

Figure 16: *Shape parametrization for the prompt (top), secondary (middle) and combinatorial component (bottom) in the impact-parameter distribution for* $p_T(D^+)$ *in the range [3.5; 4.5] GeV/c.*

fired, or not, the MB trigger. Figure 17 shows the result of the fit for candidates with $p_T(D^+) \geq 1.5$ GeV/c. We assume no p_T-dependence. We performed the fit using the same function used for the other invariant $K^-\pi^+\pi^+$ mass plots (see Sec. 5.1) but setting the two parameters of the function used for the background as common parameters. We can then evaluate the efficiency of the MB trigger, ε_{MB}, as stated in Equations 13 and 14:

$$\varepsilon_{MB} = \frac{Y_{ZB\&MB}}{Y_{ZB\&MB} + Y_{ZBnoMB}} \tag{13}$$

$$\sigma_{\varepsilon_{MB}} = \sqrt{\frac{\varepsilon_{MB} \cdot (1 - \varepsilon_{MB})}{Y_{ZB\&MB} + Y_{ZBnoMB}}} \tag{14}$$

where $Y_{ZB\&MB}$ and Y_{ZBnoMB} are the fitted signal yields in ZB events that triggered the MB L1 bit or not. In our case we obtain $\varepsilon_{MB} \simeq 1$ and $\sigma_{\varepsilon_{MB}} \simeq 0$. Equations 15 and 16 show the values we obtain.

$$\varepsilon_{MB} = \frac{646}{646 + 8} = 0.988 \tag{15}$$

$$\sigma_{\varepsilon_{MB}} = \sqrt{\frac{0.988 \cdot (1 - 0.988)}{646 + 8}} = 0.004 \tag{16}$$

This result confirms that the two subsamples (ZB and MB) can be safely added because any uncertainty is negligible with respect to the final 5–10% uncertainties on the D^+. In principle the MB trigger might be sensitive to the effects listed above also in case of events with a D^0 candidate. Since the efficiency is so high, it turns out not to be sensitive to them. We assume ε_{MB} to be 1 and treat the uncertainty as a systematic effect[4].

[4]The MB sample represents about the 43% of the total; this reduces the effect of the MB trigger inefficiency to a level of per mille.

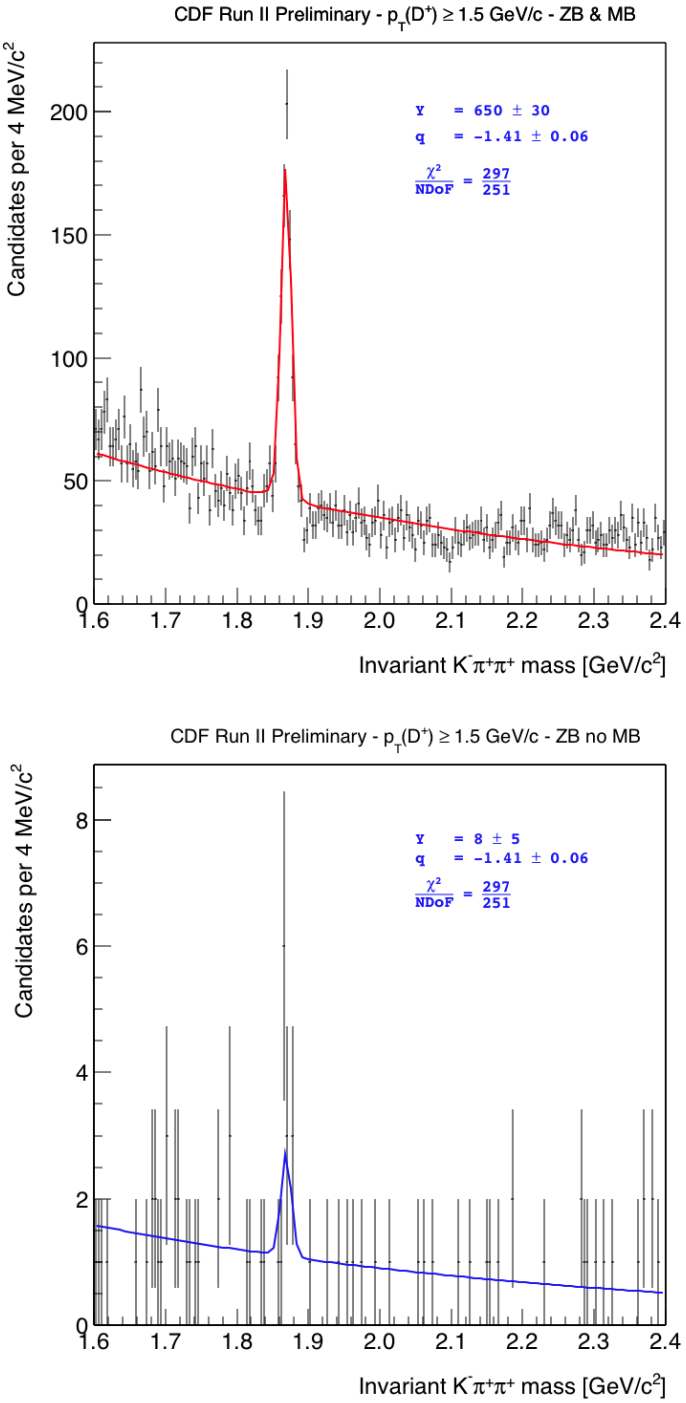

Figure 17: *Result of the combined fit of the invariant $K^-\pi^+\pi^+$ mass plots for candidates of ZB events that fired (top) or not (bottom) the MB trigger.*

6.2 Reconstruction efficiency

6.2.1 Efficiency Definition

We intend to measure the differential production cross section $d\sigma/dp_T$ of the D^+ averaged over a given p_T interval and integrated over [-1,+1] in η. To evaluate the reconstruction efficiency we use the MC sample described in Sec. 4.0.3. The denominator of the efficiency is the number of D^+ mesons produced by the MC in the appropriate η region and p_T interval with a flat η distribution and with a p_T spectrum in agreement with previous measurements. The numerator of the efficiency is the number of generated D^+ mesons that are reconstructed and pass all the analysis cuts. Note that we will have a different efficiency, in general, for even and odd events and for each transverse momentum bin.

$$\varepsilon_{rec}(p_T(D^+)) = \frac{N_{REC}(p_T(D^+))\big|_{CUTS}}{N_{GEN}(p_T(D^+))\big|_{|y|\leq 1}} \tag{17}$$

This definition of ε_{rec} represents a global reconstruction efficiency for our candidates. It accounts for the detector response, the reconstruction process and our selection criteria.

6.2.2 Description of the Method

For each p_T interval, we generate a sample of D^+ with a flat distribution in y between -1 and +1 and a transverse momentum distribution compatible with previous measurements. The D^+ is decayed into $K^-\pi^+\pi^+$ and is superimposed to an "underlying event" obtained from a simulation of "minimum bias" events weighted in such a way to reproduce the distribution of reconstructed primary vertices observed in our data sample.

Monte Carlo events generated in this way are processed by full time-dependent detector simulation and offline reconstruction, then analyzed by the same code and the same procedure as real data. In this way we obtain a D^+ yield for each p_T interval from Monte Carlo. The average efficiency is obtained separately for each p_T interval as the ratio of the D^+ yield over the number of D^+ generated. This efficiency is used to obtain the average $d\sigma/dp_T$ integrated in the [-1,+1] y interval.

One problem we need to face is the fact that we cannot completely trust the Monte Carlo to reproduce correctly the efficiency for attaching SVX hits to COT tracks. The active channels of SVX have been changing over the course of Run II in way that has not been mirrored in full detail by the simulation. Hence, we need a data-driven procedure to take this effect into account.

For this purpose we can break down the whole analysis process into three subsequent steps:

1. The three tracks from the three D^+ decay products must be reconstructed by the COT and fall within the fiducial cuts for the COT and SVX. It is important that, at this level, no information from the SVX is used in any way. We say that these tracks are "silicon-unbiased".

2. Then silicon hits are attached to COT tracks. We require that all three tracks satisfy a "silicon quality cut" which requires at least 3 longitudinal and 3 stereo hits.

3. All D^+ that pass these requirements are submitted to the analysis procedure including optimized cuts individually for each transverse momentum bin and even and odd samples. The number of D^+ found in the final plots are taken to represent the Monte Carlo yields exactly as we do in the analysis of real data.

We believe we can trust the Monte Carlo to correctly simulate steps 1 and 3 [17], but not step 2, for the reasons explained above. Therefore we assume that we can break down the efficiency ε into the product of three partial efficiencies, each one corresponding to one of the three analysis steps outlined above:

$$\varepsilon = \varepsilon_1 \times \varepsilon_2 \times \varepsilon_3 \tag{18}$$

We want to compare the value of ε_2 as predicted by the Monte Carlo to what we measure on a real-track control-sample.

To estimate ε_2 from data we need a sample of real tracks reconstructed in the COT only, silicon-unbiased, with the same distribution in parameter space as those coming from the D^+ decay in our sample.

Our first choice is reconstructed muons from a J/Ψ sample. Taking muons from the J/Ψ peak ensures that tracks are not fake. We reweigh the sample to make sure that the distribution in parameter space (η, p_T, z_0) is as similar as possible to the D^+ decay products from the MC (that is what we will need to compare to).

In order to evaluate ε_2, we need to find out which fraction of muons in the J/Ψ sample, reconstructed as COT-only tracks and falling within the fiducial cuts, pass the "silicon quality cuts". We call this fraction "single-track relative silicon-efficiency" (meaning relative to the COT).

Due to the structure of the SVX and the local nature of possible imperfections, we decided to map the relative efficiency for single tracks as a function of track parameters and time using data. We chose to parametrize the single-track relative efficiency in this way [18]:

$$\varepsilon_{rel}(p_T, z_0, \varphi_0, \theta) = \varepsilon_a(z_0, \varphi_0) \cdot \varepsilon_b(p_T) \cdot \varepsilon_c(\cot(\theta)) \tag{19}$$

Fig. 18 shows what we obtain for the three components using muons from J/Ψ. In the plots all distributions are normalized so that the value as a function of one or two parameters is the efficiency averaged over all remaining parameters.

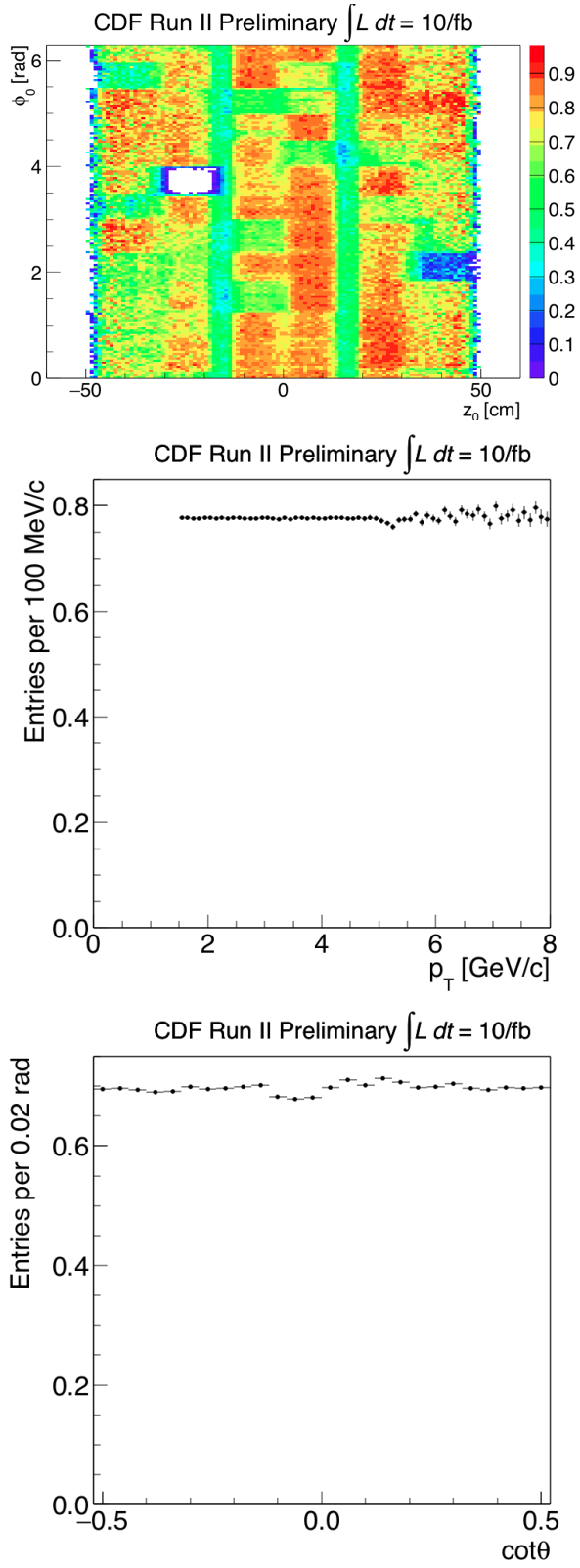

Figure 18: *Three components for the relative silicon single-track efficiency for one time period using the muons from* J/Ψ.

We note that the $\cot(\theta)$ distribution is sufficiently flat to be considered uniform and we remove it from the parametrization of the relative efficiency which then becomes:

$$\varepsilon_{rel}(p_T, z_0, \varphi_0) = \varepsilon_a(z_0, \varphi_0) \cdot \varepsilon_b(p_T) \tag{20}$$

The p_T dependent component is normalized in order to yield $< \varepsilon_b >= 1$, where the average is taken over the J/ψ sample.

The large short-distance variations of the relative efficiency are evident in the top 2D-grid of Fig. 18. This is due to individual detector element malfunctions and reflects the detailed mechanical structure of the SVX. The same plot is shown on the left side of Fig. 19 and 20 for five different time intervals during Run II. The non negligible changes with time are evident. The corresponding plots, as obtained from the Monte Carlo, are shown on the right side of Fig. 19 and 20 although with lower statistics. Small but significant discrepancies between data and Monte Carlo are apparent. This is the main reason why we need to correct the Monte Carlo efficiency using data.

We also note that we have no efficiency measurement for $p_T < 1.5$ GeV/c. This is because of the minimum momentum needed for a muon to be able to reach the CDF muon detector. Fig. 21 shows the transverse momentum distribution of D^+ decay products for different $p_T(D^+)$ bins for one time period. A significant fraction of those tracks fall below 1.5 GeV/c and, therefore, we need to extend this measurement to much lower transverse momentums.

For this purpose we use a $D^* \rightarrow \pi^+ D^0[\rightarrow K^-\pi^+]$ sample coming from the hadronic two-track trigger. We require the reconstructed decay products of the D^0 to satisfy the trigger requirements in order to remove a possible trigger bias from the π_s. The p_T distribution of the pion sample obtained in this way is shown in Fig. 22.

Plenty of tracks are present in the p_T region of interest (0.4 - 1.5 GeV/c).

The average relative efficiency as a function of p_T obtained from the π_s sample is shown in Fig. 23 compared with the one obtained for D^+ decay products from the Monte Carlo. There is a very distinct turn-on for very low p_T shown by both data and Monte Carlo. To evaluate the D^+ efficiency we need to model this turn-on correctly, given that a large fraction of the D^+ decay products fall in this region. Although the shapes appear to be very similar, the "plateau" values are significantly different.

If we look at the (z_0, η) distribution of the π_s in Fig. 24, we see that it is clearly reminiscent of the SVX barrel structure and that means that this sample cannot be considered silicon-unbiased. The reason can be traced to the very strong correlation between the direction of the π_s and the direction of the D^0 decay products. The D^0 decay products are tracks reconstructed by the SVT (Silicon Vertex Trig-

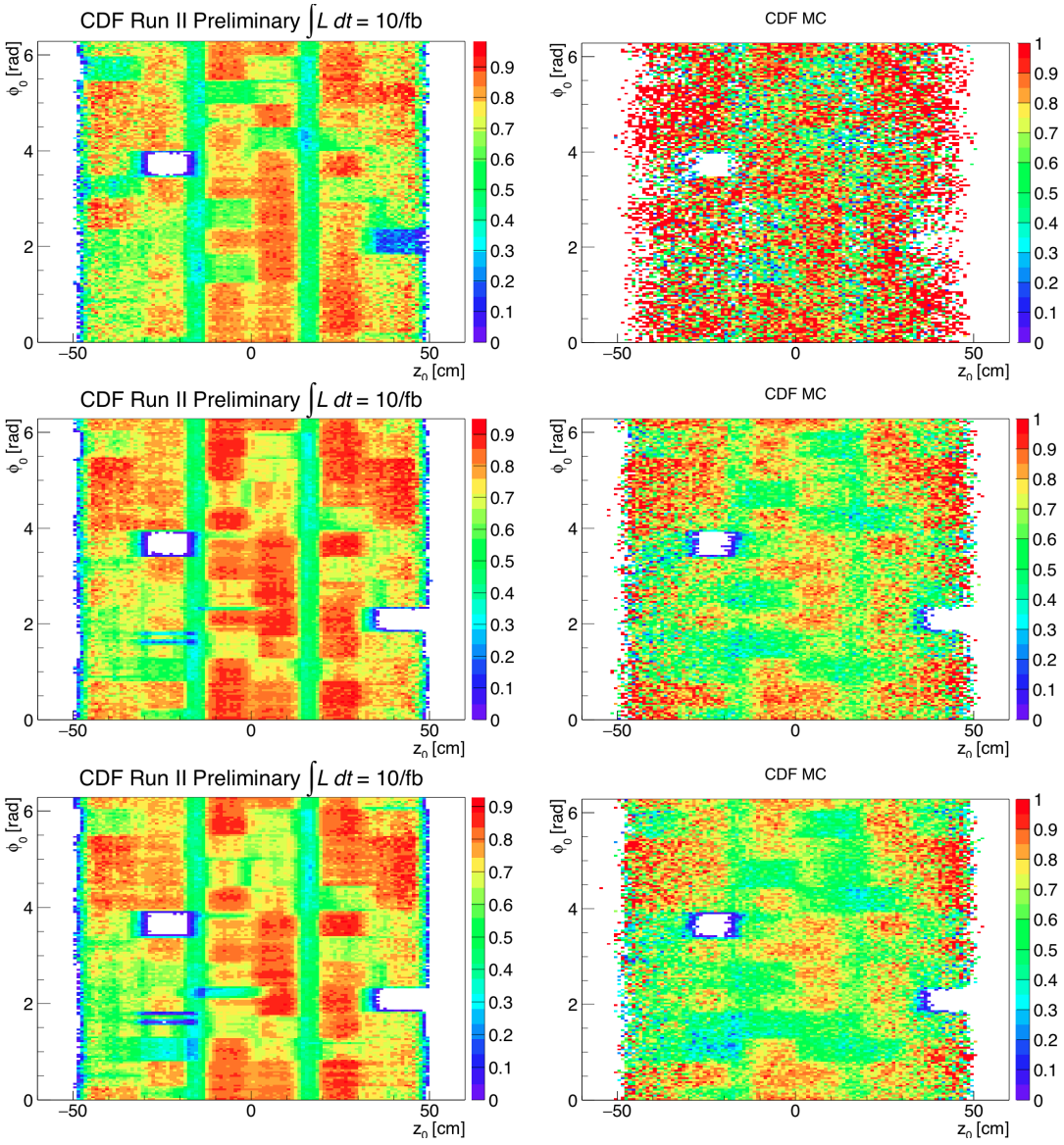

Figure 19: *(z_0, ϕ_0)-component for the relative silicon single-track efficiency for the first three time periods using the muons from J/Ψ (left) and the MC decay tracks of the D^+ (right).*

ger) trigger which requires high silicon efficiency. This causes the π_s distribution to be more dense in the regions of higher silicon efficiency. For example there is a very clear depletion of the track density close the dead region corresponding to the barrel-to-barrel gaps. This significant bias of the π_s distribution towards detector regions of higher efficiencies, will cause an overestimate of the average

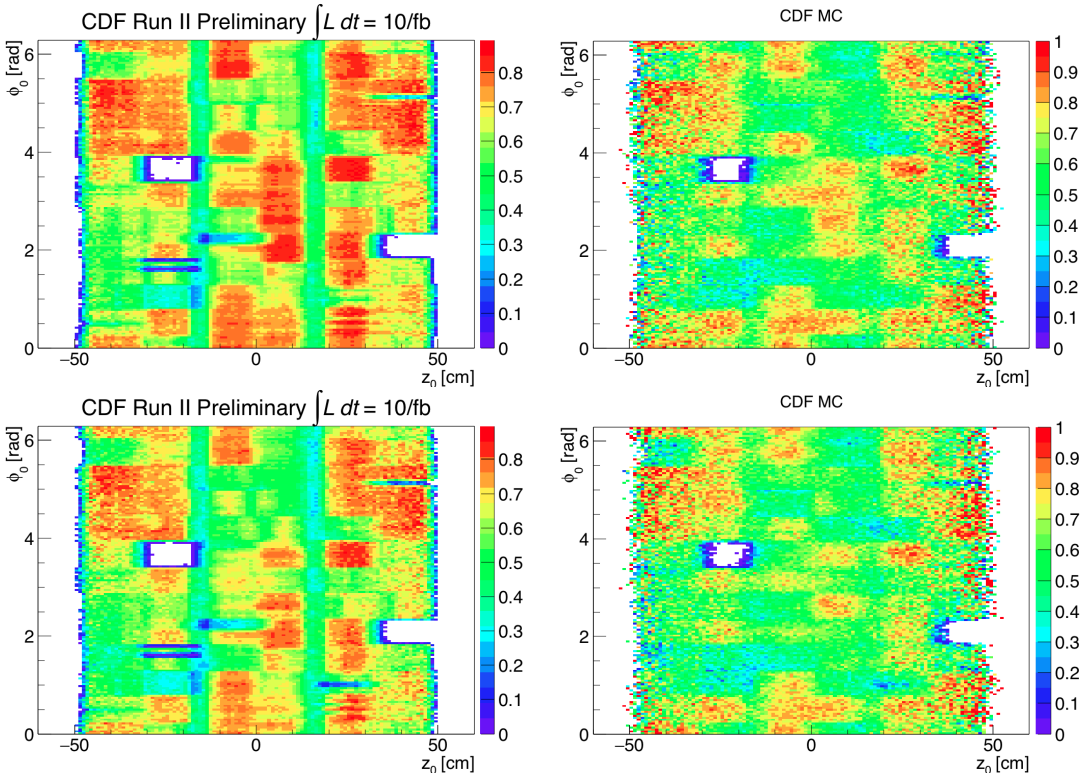

Figure 20: *(z_0, ϕ_0)-component for the relative silicon single-track efficiency for the first three time periods using the muons from J/Ψ (left) and the MC decay tracks of the D^+ (right).*

relative silicon efficiency. It is no surprise that it turns out to be higher than the same quantity estimated from D^+ Monte Carlo or from real muons from J/Ψ, as shown in Fig. 23.

Given the evidence at hand, we chose to use the relative efficiency obtained from the truly silicon-unbiased J/Ψ sample to build the (z_0, φ_0)-grid and for the value of the plateau at high p_T and model the turn on at low p_T from the relative efficiency obtained from the π_s sample, scaled down to match the J/Ψ plateau.

We perform a single fit of the relative efficiency as a function of p_T with the following, three-parameter analytical expression:

$$\varepsilon_b(p_T) = C - a \cdot e^{-b \cdot p_T} \tag{21}$$

One additional free parameter (Scale) is added in the fit as a global scale factor for the π_s points. The results for the five time periods are shown in Fig. 25. Values of the parameters are listed in Table 4.

Our final parametrization of the single-track relative efficiency is obtained as

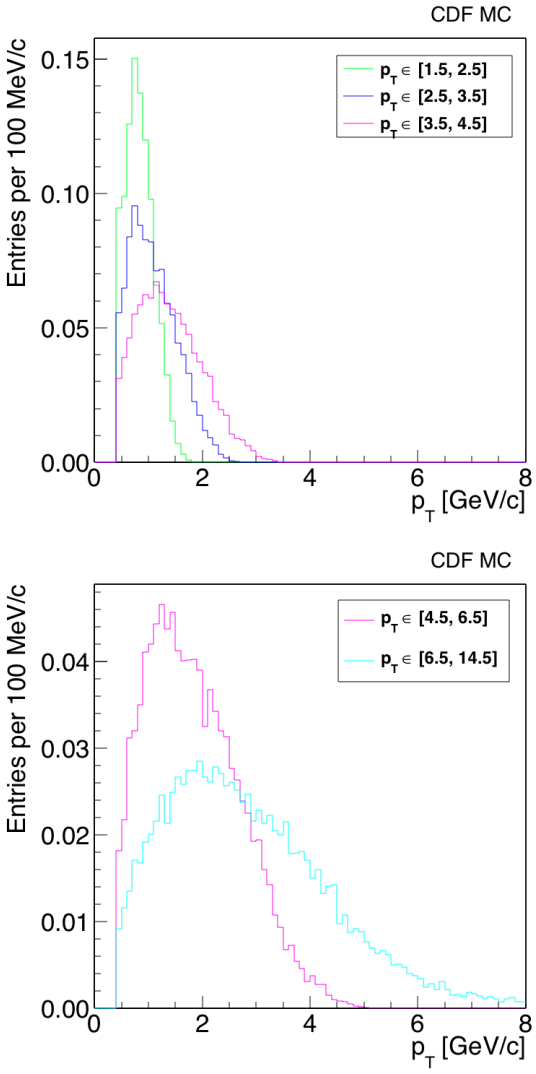

Figure 21: *Transverse momentum distribution of D^+ decay products for different $p_T(D^+)$ bins for one time period.*

the product of the $\varepsilon_a(z_0, \varphi_0)$-grid times the turn-on fitted function $\varepsilon_b(p_T)$, each taken from one of the five different time periods.

Now we have all we need to estimate ε_2 from the data.

We assume that the single track detection efficiencies for the three decay products are uncorrelated functions of individual track parameters and, therefore, ε_2 is calculated as the product of the three relative efficiencies obtained by applying the single-track maps to the three decay tracks separately. This accounts for the effect of correlations among tracks due to the kinematics of D^+ decay, We take all the

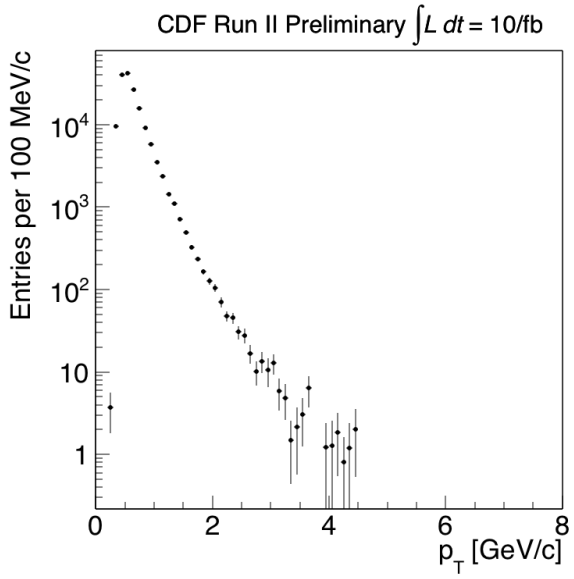

Figure 22: p_T *distribution for the* π_s *for one time period.*

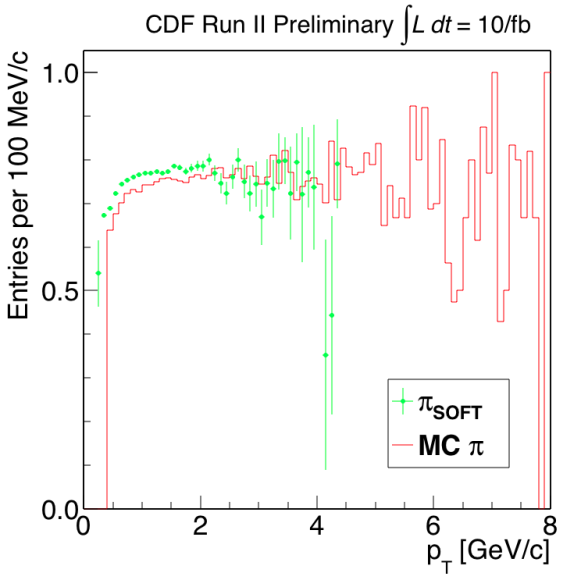

Figure 23: p_T *distribution for the* π_s *and for the MC* π *for one time period.*

D^+ in the Monte Carlo which pass step 1 and for each one of the three decay tracks we use our parametrization to obtain an estimate of the relative time-dependent silicon efficiency for that track. We take the product of the three relative efficiencies as an estimate of the relative efficiency for that particular D^+, and the average

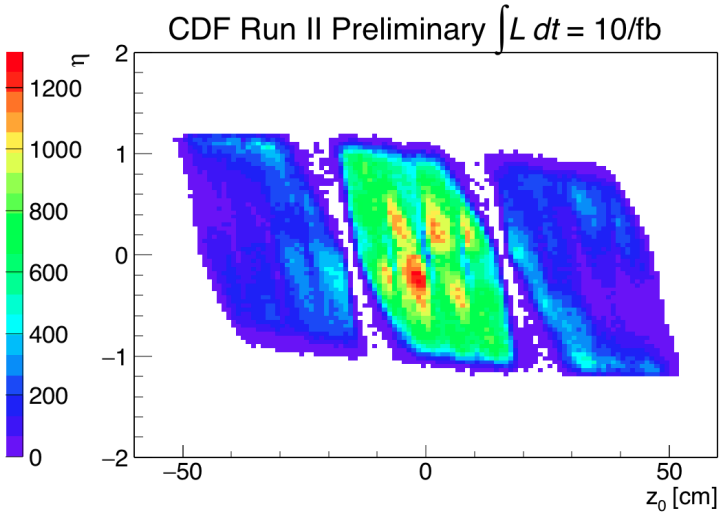

Figure 24: *(z_0, η) distribution of the π_s for one time period.*

Data-taking Period	Scale	C	a	b
0	0.8750 ± 0.0003	0.888 ± 0.004	0.42 ± 0.04	3.52 ± 0.28
1	0.89148 ± 0.00018	0.8780 ± 0.0016	0.45 ± 0.14	3.42 ± 0.10
2	0.86541 ± 0.00015	0.8683 ± 0.0017	0.42 ± 0.13	3.25 ± 0.10
3	0.85644 ± 0.00012	0.8464 ± 0.0013	0.48 ± 0.14	3.48 ± 0.08
4	0.84610 ± 0.00019	0.8150 ± 0.0018	0.44 ± 0.14	3.11 ± 0.08

Table 4: *Results of the fit to the p_T-efficiency distribution for all the five data-taking periods.*

value over all D^+ which pass step 1 as an estimate of ε_2 from the data.

Following exactly the same strategy, but using the MC to build the (z_0, φ_0)-grid and to model the p_T function, we define ε_2 from the Monte Carlo. Finally we define a correction factor (CF) as:

We then repeat exactly the same procedure as described above substituting the efficiency maps obtained with the J/ψ plus D^* samples, with efficiency maps, obtained in the same way, but using the decay products of the D^+ from the Monte Carlo. In this way we obtain two different determinations of ε_2, one with data, and one with Monte Carlo and we can derive a Correction Factor (CF) from the ratio of the two.

$$CF = \varepsilon_2(\text{from data})/\varepsilon_2(\text{from Monte Carlo}) \tag{22}$$

Correction factors for the five different p_T bins are listed in Table 5.

We use CFs to correct the efficiencies obtained from the Monte Carlo:

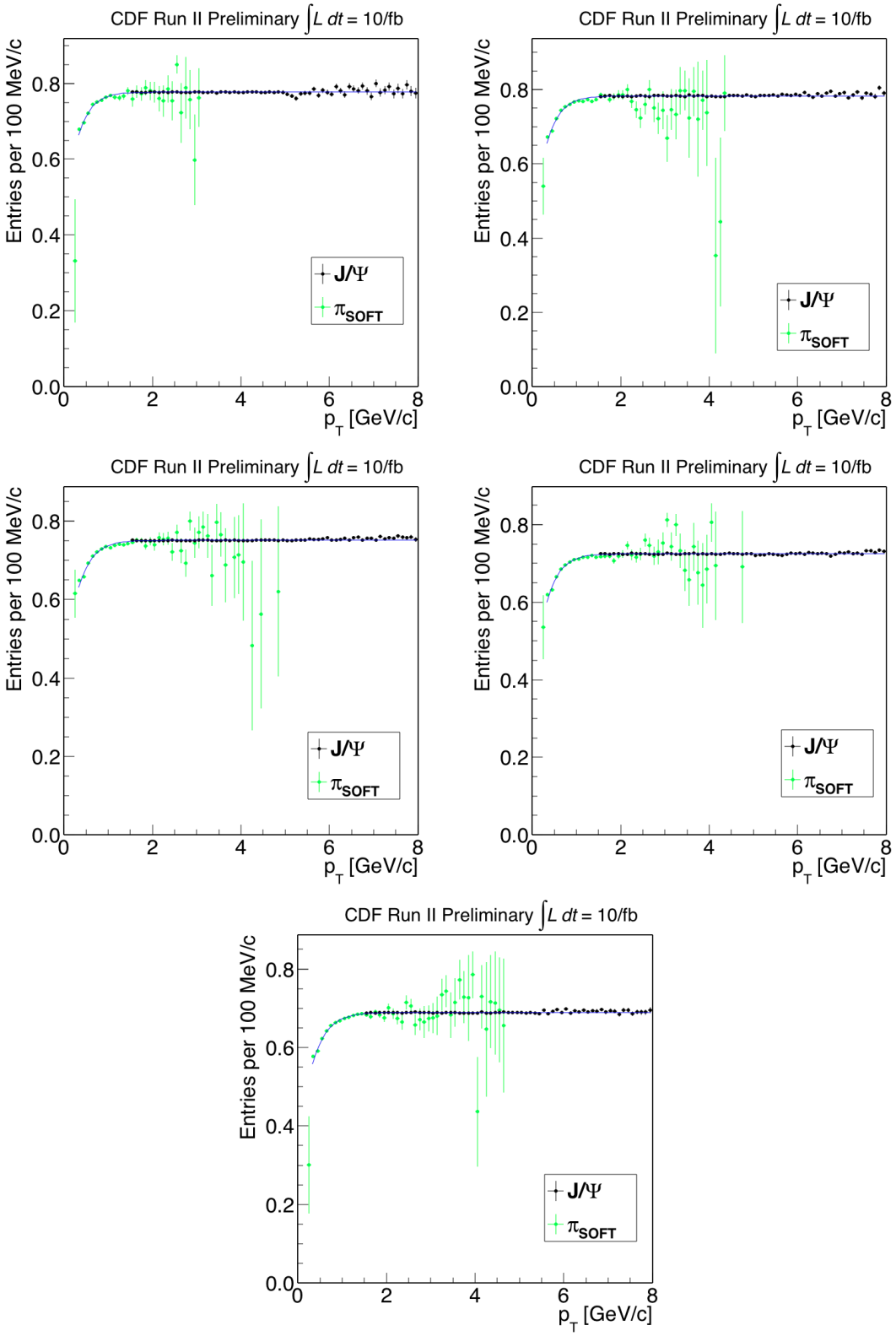

Figure 25: *Fit to the p_T-efficiency of the π_s and μ for all the time periods.*

$p_T(D^+)$ [GeV/c]	CF
[1.5; 2.5]	1.15 ± 0.12
[2.5; 3.5]	1.19 ± 0.12
[3.5; 4.5]	1.20 ± 0.13
[4.5; 6.5]	1.22 ± 0.13
[6.5; 14.5]	1.25 ± 0.13

Table 5: *Correction factors as a function of* $p_T(D^+)$.

$$\text{corrected efficiency} = (\text{MC efficiency}) \cdot CF \tag{23}$$

This is done separately for each p_T bin. Table 9 lists the efficiencies from MC, the correction factors (CF) and the data-corrected efficiencies (ε_{corr}) for each p_T bin and even and odd samples. Note that the same CF applies to both even and odd data samples since analysis cuts, which may be different for even and odd samples, are applied only in step 3 and can only have an effect on ε_3.

$p_T(D^+)[GeV/c]$	Subsample	$\varepsilon_{MC}[\%]$	$\varepsilon_{corr}[\%]$	CF
[1.5; 2.5]	Even	0.261 ± 0.010	0.30 ± 0.030	1.15 ± 0.12
	Odd	0.230 ± 0.009	0.264 ± 0.029	
[2.5; 3.5]	Even	1.073 ± 0.025	1.28 ± 0.13	1.19 ± 0.12
	Odd	0.996 ± 0.024	1.18 ± 0.12	
[3.5; 4.5]	Even	2.054 ± 0.047	2.46 ± 0.27	1.20 ± 0.13
	Odd	2.029 ± 0.047	2.43 ± 0.27	
[4.5; 6.5]	Even	3.813 ± 0.072	4.65 ± 0.50	1.22 ± 0.13
	Odd	3.882 ± 0.073	4.74 ± 0.51	
[6.5; 14.5]	Even	7.35 ± 0.15	9.19 ± 0.90	1.25 ± 0.13
	Odd	7.23 ± 0.15	9.04 ± 0.91	

Table 6: *Reconstruction efficiency as a function of* $p_T(D^+)$.

In 11 we list the selection requirements applied to the $D^* \to \pi^+ D^0[\to K^-\pi^+]$ and J/Ψ samples.

7 Systematic uncertainties

7.1 Luminosity

As we discussed in Section 3.3 the measured trigger luminosity is obtained through the extrapolation of the total $p\bar{p}$ cross section from the measured value at $\sqrt{s} = 1.8$ TeV during the Run I; the systematic uncertainty associated to this extrapolation is assessed in [19] to be $\sigma^{SYS}_{L_{trig}} = 5.8$ %.

7.2 Yield

Sec. 5 describes how we perform the two-dimensional fit to determine the signal yield. Each pdf used in the fit could be a possible source of systematic uncertainty: prompt and secondary shapes, and combinatorial backgorund.

To assess the possible variations to the final results due to a mismodeling of the signal shapes, we have repeated the invariant mass fits of the yields adding another gaussian. The variations, ΔY_{sig}, from the measured values are taken as systematic uncertainties.

For the combinatorial background, instead, we have repeated the fits using an exponential instead of a second-order polynomial function.
The variations, ΔY_{bkg}, from the measured values are taken as systematic uncertainties.
Table 7 summarizes the numbers obtained for ΔY_{sig} and ΔY_{bkg}; $\sigma^{SYS}_{mass-shape}$ is the sum in quadrature of the two contributions.

$p_T(D^+)$ [GeV/c]	Subsample	ΔY_{sig}	ΔY_{bkg}	$\sigma^{SYS}_{mass-shape}$
[1.5; 2.5]	Even	0.024%	0.15%	0.15%
	Odd	0.020%	0.052%	0.056%
[2.5; 3.5]	Even	0.017%	0.023%	0.029%
	Odd	0.015%	0.10%	0.10%
[3.5; 4.5]	Even	0.050%	0.034%	0.060%
	Odd	0.052%	0.030%	0.060%
[4.5; 6.5]	Even	0.042%	0.13%	0.14%
	Odd	0.038%	0.092%	0.10%
[6.5; 14.5]	Even	0.056%	0.60%	0.60%
	Odd	0.058%	0.048%	0.075%

Table 7: *Systematic uncertainties related to the yield measurement: variation of the mass shape.*

We also evaluate the possible variations to the final results due to a mismodeling

in the impact-parameter distributions. We have repeated the impact-parameter fits of the yields adding another gaussian to the prompt or to the secondary or to the combinatorial parameterization. The variations, ΔY_{prompt}, ΔY_{sec} and ΔY_{comb} from the measured values are taken as systematic uncertainties.
Table 8 summarizes the numbers obtained for ΔY_{prompt}, ΔY_{sec} and ΔY_{comb}; $\sigma^{SYS}_{ImpPar-shape}$ is the sum in quadrature of the two contributions.
Table 7 summarizes the numbers obtained for ΔY_{sig} and ΔY_{bkg}; $\sigma^{SYS}_{mass-shape}$ is the sum in quadrature of the three contributions.

$p_T(D^+)$ [GeV/c]	Subsample	ΔY_{prompt}	ΔY_{sec}	ΔY_{comb}	$\sigma^{SYS}_{ImpPar-shape}$
[1.5; 2.5]	Even	0.05%	0.020%	0.10%	0.11%
	Odd	0.06%	0.09%	0.13%	0.17%
[2.5; 3.5]	Even	0.20%	0.05%	0.04%	0.21%
	Odd	0.15%	0.07%	0.07%	0.18%
[3.5; 4.5]	Even	0.03%	0.08%	0.10%	0.13%
	Odd	0.021%	0.03%	0.09%	0.10%
[4.5; 6.5]	Even	0.12%	0.09%	0.04%	0.16%
	Odd	0.14%	0.04%	0.04%	0.15%
[6.5; 14.5]	Even	0.06%	0.13%	0.07%	0.16%
	Odd	0.07%	0.15%	0.06%	0.18%

Table 8: *Systematic uncertainties related to the yield measurement: variation of the impact-parameter shape.*

In Table 11 we show σ^{SYS}_{shape} which is the sum in quadrature of $\sigma^{SYS}_{mass-shape}$ and $\sigma^{SYS}_{ImpPar-shape}$. We find this effect negligible.

7.3 Trigger efficiency

As described in Section 6.1 we measured the efficiency of the `MINBIAS` trigger to be (98.8 ± 0.4) %; we have assumed it to be 1 when summing the ZB and the MB subsample in the analysis and we treat the 0.4 % as a systematic uncertainty on this assumption. Because the MB sample is the 43 % of the total, the final final uncertainty on the measurement is $\sigma^{SYS}_{\varepsilon_{trig}} = 0.04 \cdot 0.43 = 0.17\%$.

7.4 Reconstruction efficiency

Section 6.2 describes how we evaluate the reconstruction efficiency. In order to have a feeling for the importance of the correlations in the efficiency as a function of track parameters which we have partially integrated in building the efficiency

maps, we compare the correction factors obtained with the Monte Carlo using the maps as explained in section 6.2.2and without using the maps, directly from simulation, that is taking directly the number of D^+ which pass the SVX quality cuts according to the MC and divide by the total number passing step 1 of the analysis. In this way we obtain a new correction factor with respect to ε_2 obtained from the data (CF2). In absence of correlations the two correction factors should be the same. They are shown side by side in Table 9. Pessimistically we can interpret the discrepancies between the two columns as a limit of our understanding of the effect of correlations and translate them into a contribution to systematic errors. For lack of arguments on which of the two columns we should prefer, we take the average of the two (CF - third column) as the central value and half of the difference as the sitematic error.

$p_T(D^+)$ [GeV/c]	CF(1)	CF(2)	CF	$\Delta\varepsilon_{rec}^{SYS}$ [%]
[1.5; 2.5]	1.15 ± 0.12	1.154 ± 0.044	1.154 ± 0.041	0.20
[2.5; 3.5]	1.19 ± 0.12	1.209 ± 0.050	1.206 ± 0.046	1.0
[3.5; 4.5]	1.20 ± 0.13	1.287 ± 0.052	1.275 ± 0.048	4
[4.5; 6.5]	1.22 ± 0.13	1.391 ± 0.055	1.365 ± 0.051	8
[6.5; 14.5]	1.25 ± 0.13	1.500 ± 0.058	1.458 ± 0.052	12

Table 9: *Systematic uncertainties related to the reconstruction efficiency measurement.*

Table 10 lists the efficiency from the MC, the final correction factor (CF) and the data-corrected efficiency (ε_{corr}) for each p_T bin and even and odd subsamples.

$p_T(D^+)[GeV/c]$	Subsample	ε_{MC}[%]	ε_{corr}[%]	CF
[1.5; 2.5]	Even	0.261 ± 0.010	0.302 ± 0.017	1.154 ± 0.041
	Odd	0.230 ± 0.009	0.266 ± 0.015	
[2.5; 3.5]	Even	1.073 ± 0.025	1.29 ± 0.06	1.206 ± 0.046
	Odd	0.996 ± 0.024	1.20 ± 0.05	
[3.5; 4.5]	Even	2.054 ± 0.047	2.61 ± 0.12	1.275 ± 0.048
	Odd	2.029 ± 0.047	2.59± 0.11	
[4.5; 6.5]	Even	3.813 ± 0.072	5.20 ± 0.22	1.365 ± 0.051
	Odd	3.882 ± 0.073	5.30 ± 0.22	
[6.5; 14.5]	Even	7.35 ± 0.15	10.7 ± 0.4	1.458 ± 0.052
	Odd	7.23 ± 0.15	10.5 ± 0.4	

Table 10: *Reconstruction efficiency as a function of* $p_T(D^+)$.

7.5 Total systematic uncertainties

Table 11 summarizes the systematic uncertainties described in the previous sections; the last column is the sum in quadrature of all the contributions.

$p_T(D^+)$ [GeV/c]	$\sigma^{SYS}_{L_{trig}}$ [%]	σ^{SYS}_{shape} [%]	$\sigma^{SYS}_{\varepsilon_{trig}}$ [%]	$\sigma^{SYS}_{\varepsilon_{rec}}$ [%]	σ^{SYS}_{TOT} [%]
[1.5; 2.5]	5.8	E:0.19/O:0.18	0.17	0.20	6
[2.5; 3.5]	5.8	E:0.21/O:0.21	0.17	1.0	6
[3.5; 4.5]	5.8	E:0.14/O:0.12	0.17	4	7
[4.5; 6.5]	5.8	E:0.21/O:0.18	0.17	8	10
[6.5; 14.5]	5.8	E:0.62/O:0.20	0.17	12	13

Table 11: *Systematic uncertainties summary and final total values.*

8 Differential Cross-Section

Putting together all the ingredients needed in Equation 1 we can evaluate the measured differential cross sections for each bin of p_T and even/odd subsamples. Table 12 shows the results with statistical errors only. Values obtained with even/odd samples are well in agreement. Table 13 shows the cross sections for all p_T bins, averaged over even/odd samples, with statistical errors and systematic errors obtained as discussed in the previous sections.

$p_T(D^+)[GeV/c]$	Subsample	$d\sigma/dp_T[nb/GeV/c]$	Δ/σ
[1.5; 2.5]	Even	77,000 ± 19,000	0.4
	Odd	64,000 ± 21,000	
[2.5; 3.5]	Even	38,800 ± 3,800	0.4
	Odd	35,000 ± 4,200	
[3.5; 4.5]	Even	15,800 ± 1,700	0.7
	Odd	16,000 ± 1,700	
[4.5; 6.5]	Even	5,040 ± 450	0.05
	Odd	5,010 ± 450	
[6.5; 14.5]	Even	443 ± 44	1.4
	Odd	530 ± 46	

Table 12: *Differential Cross Sections for Even/Odd samples*

8.0.1 Time

To test the stability of the complete procedure, we divide out data into five different time periods along the 10-year duration of Run II and repeat the measurement of the differential cross section in each p_T bin for each time period separately. Given the large variations of the instantaneous luminosity, and of the running conditions in general, we believe this to be a very stringent test of the performance of the method used in this analysis. The first bin, $p_T(D^+)\ \epsilon\ [1.5;\ 2.5]$ GeV/c, is not included in this study because of not sufficient statistics.

Results are shown in Figures 26 and 27. No significant time-dependence is observed. The time-independent hypothesis yields a total χ^2 of 15 for 16 degrees of freedom. There is no systematic uncertainty related to the time dependence.

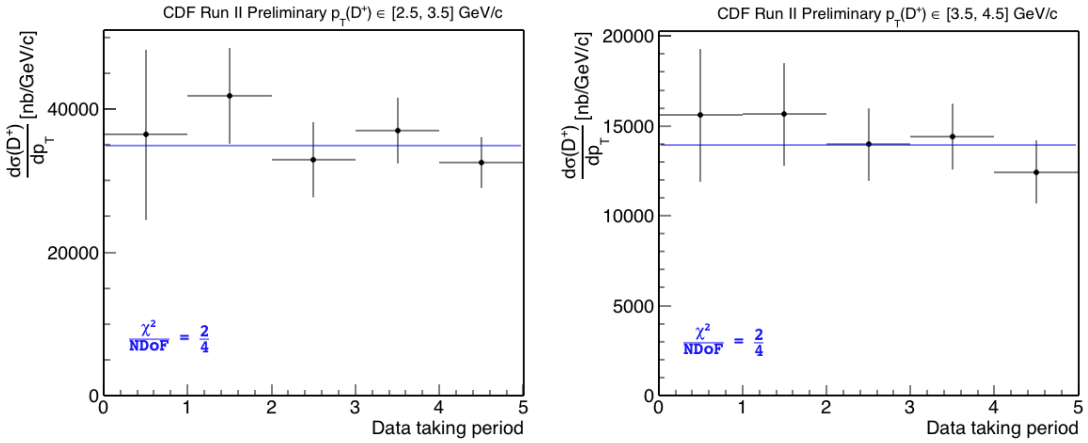

Figure 26: *D^+ production cross section as a function of data taking periods.*

9 Comparison with Previous Results

We can compare our result to the previous CDF published measurement [1]. It is difficul to compare directly the two measurements because of the different bin widths used in the two analyses. , We have compared both results to a FONLL prediction [20] as shown in Figure 31. The theoretical prediction seems to overestimate the measurements.

We note the importance of the reconstruction efficiency correction applied on the MC sample. In Figure 30 we show the comparison with the CDF published measurement and ours, if we do correct or we do not. Without applying such a correction, they disagree in the overlapping region.

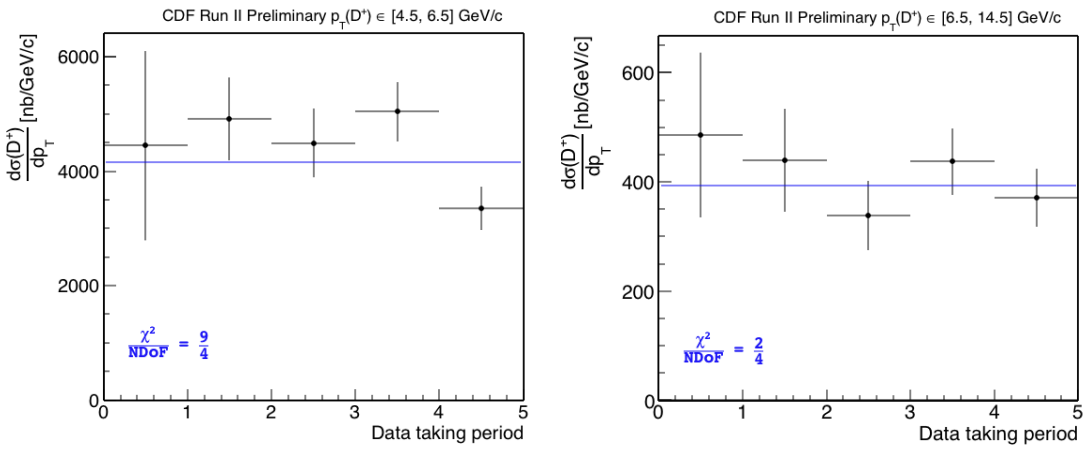

Figure 27: *D^+ production cross section as a function of data taking periods.*

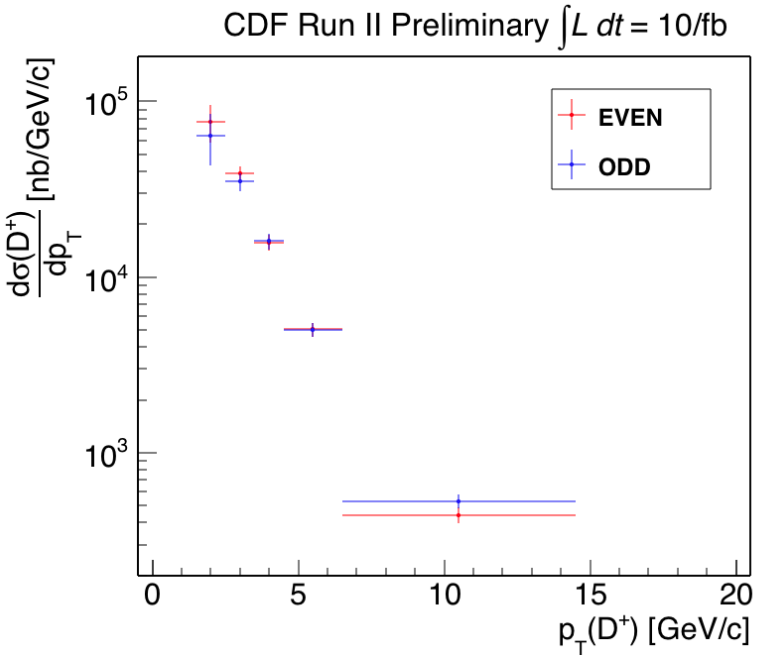

Figure 28: *Measured D^+ production cross section as a function of $p_T(D^+)$ for even-numbered and odd-numbered events: log scale.*

10 Conclusions

We have presented a study of the production of D^+ mesons using data collected by the `ZEROBIAS` and the `MINBIAS` triggers. We have measured the differential production cross section as a function of the transverse momentum down to $p_T =$

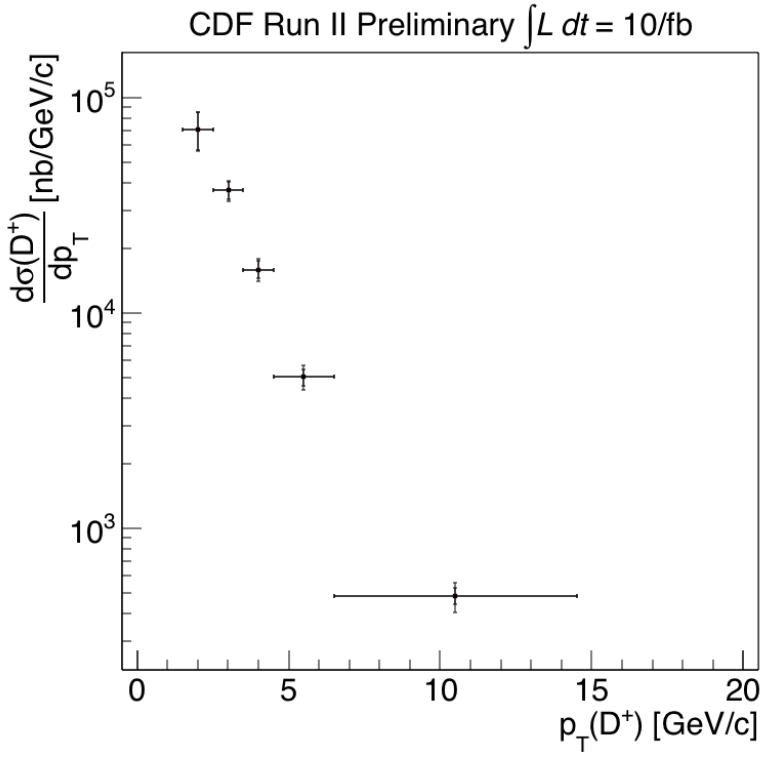

Figure 29: *Measured D^+ production cross section as a function of $p_T(D^+)$: log scale.*

1.5 GeV/c.

This work presents the first measurement of the differential production cross section of this charmed meson to very low $p_T(D^+)$ values at TeV $p\bar{p}$ collider energies.

Recently, other measurements of charm production cross section at low-p_T became available from the ALICE and LHCb experiments at the CERN LHC proton-proton collider. However, the present measurement maintains its uniqueness in terms of initial state ($p\bar{p}$) and center-of-mass energy ($\sqrt{s}$ = 1.97 TeV). Different processes within the regions we probed can occur at different energy scales: the comprehension of the energy dependence in non-pQCD is one of the most important open questions to solve.

Our result is in agreement with the published CDF II measurement [1] within 1.7 σ. This gives us the complete p_T spectum of the D^+ production from $p_T(D^+)$

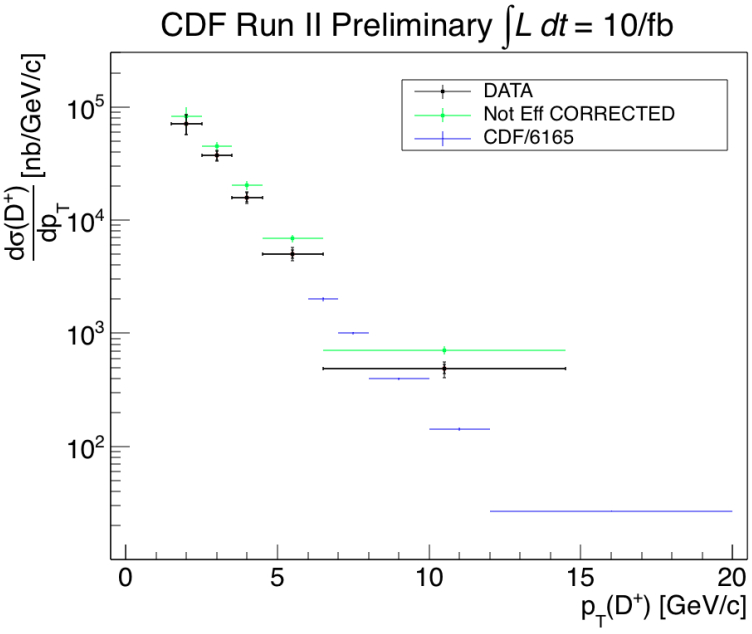

Figure 30: *Efficiency-corrected (black), not efficiency-corrected (green) and CDF published (blue) D^+ production cross section as a function of $p_T(D^+)$.*

$= 1.5$ GeV/c to $p_T(D^+) = 20$ GeV/c.

11 Appendix

11.0.1 D* Sample Selection

The "good" COT tracks in the TTT hadronic sample are selected as follows (see Table 14 for the complete list of cuts used for this sample):

- we select the $D^0 \to K\pi$ candidates with an invariant $\pi\pi$ mass within [1.7; 1.8] GeV/c^2;
- we plot the invariant mass of the selected D^0 plus a third track reconstructed in the COT only
- we determine the p_T distribution of π_s candidates under the D^{*+} peak ([2.009; 2.012] GeV/c^2), before and after the requirement of SVX hits. The ratio of the two distributions yields the average efficiency as a function of p_T

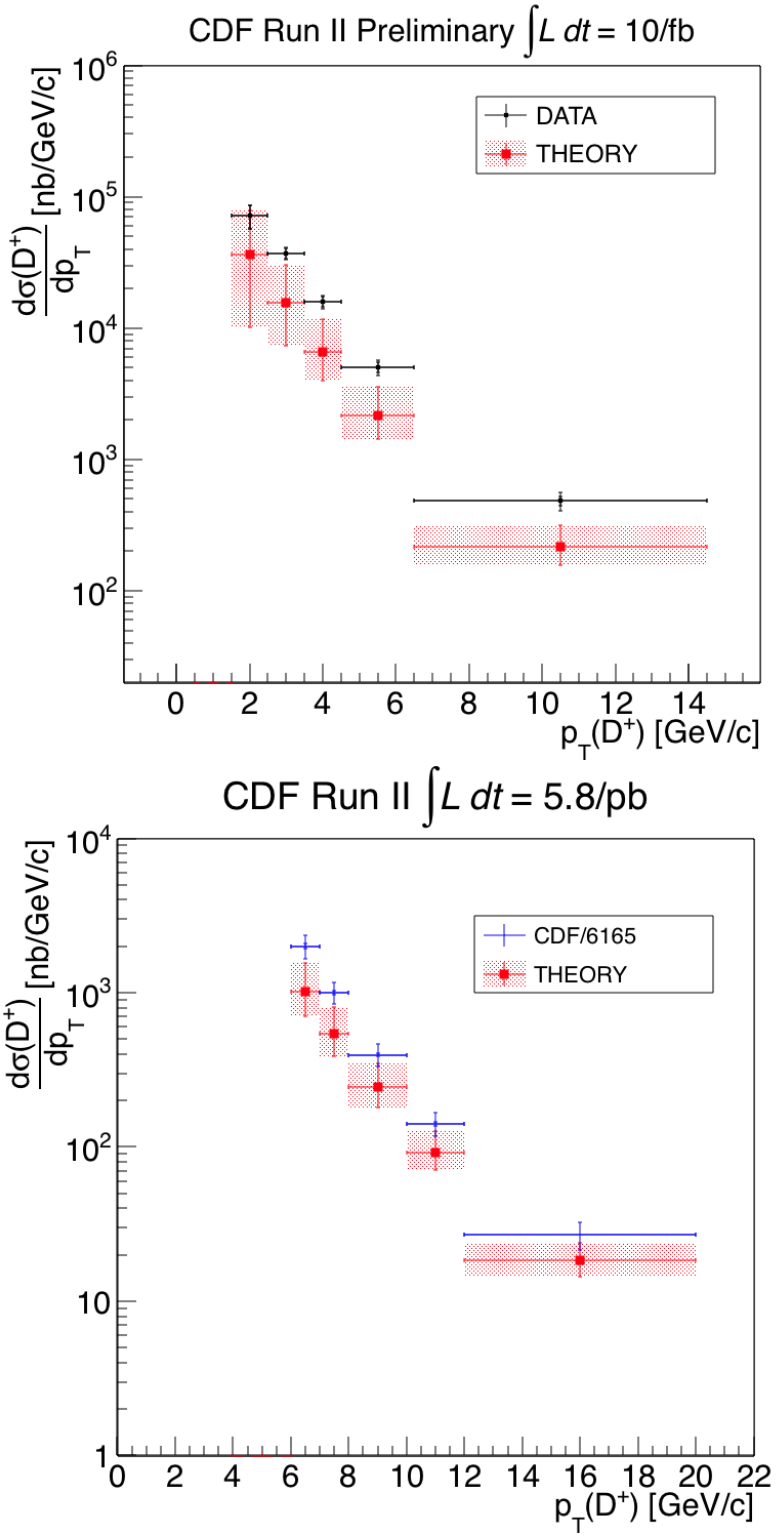

Figure 31: *Measured (left) and CDF published (right) D^+ production cross section as a function of $p_T(D^+)$ compared to FONLL prediction.*

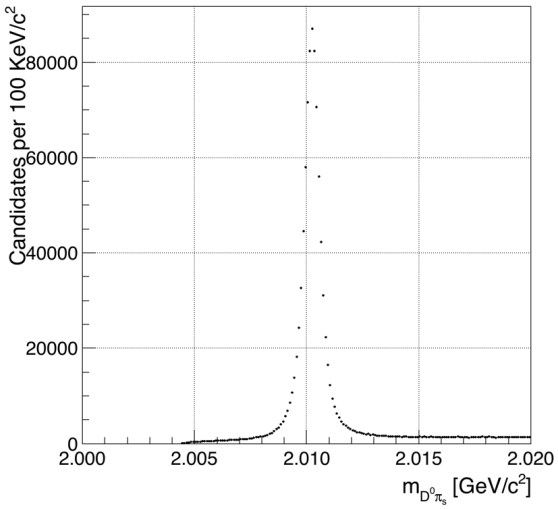

Figure 32: *Invariant $D^0\pi_s$ mass distribution of the D^{*+} candidates in the TTT hadronic sample (with the SVX requirements).*

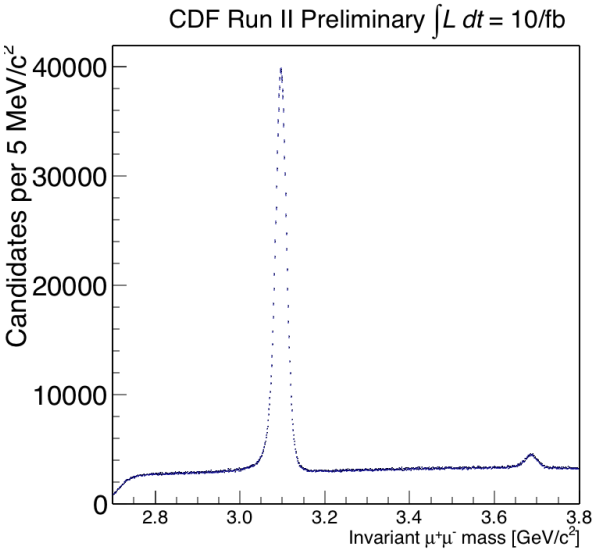

Figure 33: *Invariant $\mu^+\mu^-$ mass distribution in the J/Ψ sample (with the SVX requirements).*

11.0.2 J/Ψ Sample Selection

The "good" COT tracks in the J/Ψ sample are selected as follows (see Table 15 for the complete list of cuts used for this sample):

- we compute the invariant of all the possible pairs of tracks reconstructed in the COT only and compatible with being a $\mu\mu$ pair from J/Ψ decay;
- we select J/Ψ candidates 2σ around the peak, in the interval [3.073; 3.121] GeV/c^2;
- we also select the candidates in two side bands of the J/Ψ peak, in the intervals [3.073; 3.013] GeV/c^2 and [3.147; 3.181] GeV/c^2;
- We determine the p_T distributions of muons under the J/Ψ peak before and after applying the SVX requirements. The ratio of the two distributions yields the average efficiency as a function of p_T. The p_T distributions are sideband subtracted.

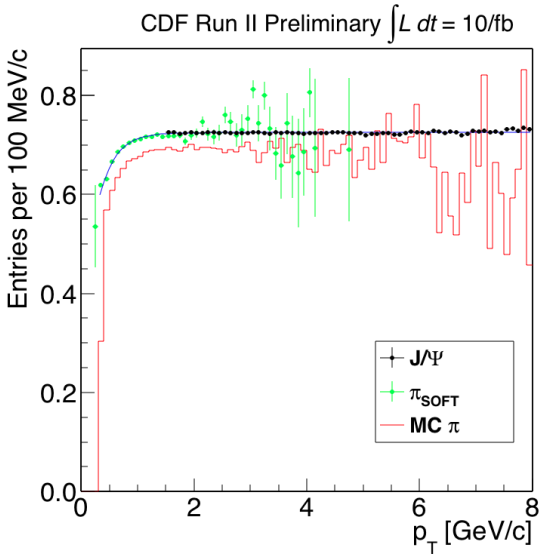

Figure 34: *Reconstruction efficiency as a function of p_T of the π_{soft} (green markers), J/Ψ (black markers) and MC (red line) for the third data-taking period.*

References

[1] D. Acosta *et al.* [CDF Collaboration], Phys. Rev. Lett. **91**, 241804 (2003).

[2] B. A. Kniehl, G. Kramer, I. Schienbein and H. Spiesberger, AIP Conf. Proc. 792, 867 (2005).

[3] B. A. Kniehl, G. Kramer, I. Schienbein and H. Spiesberger, Phys. Rev. Lett. **96**, 012001 (2006).

[4] http://www.lpthe.jussieu.fr/ cacciari/fonll/fonllform-5.html

[5] The ALICE Collaboration, arXiv:1201.0729v1 [nucl-ex], (2012).

[6] C.Chen, R. Oldeman and J. Kroll, CDF Note 5859, (2002).

[7] D. Acosta *et al.* [CDF Collaboration], Phys. Rev. Lett. **D 50**, 5518 (1994).

[8] S. Klimenko, J. Konigsberg and T. Liss, CDF Note 6314, (2003).

[9] D. Acosta *et al.*, CDF Note 6165, (2003).

[10] D. Tonelli *et al.*, CDF Note 9509, (2008).

[11] J.Appel, M.Mussini and D.Tonelli, CDF Note 11044, (2013).

[12] C. Chen, I. Cho, C. Hays, M. Herndon, J. Kraus, J. Kroll, T. Miao, P. Murat, R.Oldeman and J.C. Yun, CDF Note 6394.

[13] Jonathan Lewis, private communication.

[14] D. Acosta, S. Klimenko, J. Konigsberg, A. Madorsky, A. Nomerotski, A. Sukhanov, D. Tsybychev and S.M. Wang, CDF Note 5861.

[15] D. Acosta, R. Field, S. Klimenko, J. Konigsberg, G. Lungu, V. Necula, A. Pronko, A. Sukhanov, D. Tsybychev and S.M. Wang, CDF Note 6054.

[16] N. Moggi and F. Rimondi, CDF Note 8594.

[17] C. Chen *et al.* CDF Note 6394.

[18] C. Chen, R. Oldeman and J. Kroll CDF Note 6165.

[19] S.Klimenko and J.Konigsberg, CDF Note 6314.

[20] M. Cacciari, S. Frixione, M. L. Mangano, P. Nason and G. Ridolfi, "QCD analysis of first b cross section data at 1.96-TeV," JHEP **0407** (2004) 033.

CDF Note 11173.

$p_T(D^+)$ [GeV/c]	Subsample	[1.5; 2.5]	[2.5; 3.5]	[3.5; 4.5]	[4.5; 6.5]	[6.5; 14.5]
$N_{D^+} + N_{D^-}$	Even	170	365	304	381	282
	Odd	125	304	301	386	328
stat (%)	Even	40(24)	27(7)	28(9)	29(8)	24(8)
	Odd	40(32)	34(11)	28(9)	29(8)	27(8)
syst (%)	Even	0.32(0.19)	0.77(0.21)	0.42(0.14)	0.80(0.21)	1.7(0.62)
	Odd	0.22(0.18)	0.64(0.21)	0.36(0.12)	0.69(0.18)	0.66(0.20)
L [(nb)$^{-1}$]		16.03	16.03	16.03	16.03	16.03
stat (%)		-	-	-	-	
syst (%)		0.93(5.8)	0.93(5.8)	0.93(5.8)	0.93(5.8)	0.93(5.8)
$\varepsilon_{\text{trig}}$		1	1	1	1	1
stat (%)		-	-	-	-	
syst (%)		(0.17)	(0.17)	(0.17)	(0.17)	(0.17)
ε_{rec} [%]	Even	0.302	1.29	2.61	5.20	10.7
	Odd	0.266	1.20	2.59	5.30	10.5
stat (%)	Even	0.017(6)	0.06(5)	0.12(4)	0.22(4)	0.4(4)
	Odd	0.015(6)	0.05(4)	0.11(4)	0.22(4)	0.4(4)
syst (%)	Even	0.00060(0.20)	0.013(1.0)	0.10(4)	0.42(8)	1.3(12)
	Odd	0.00053(0.20)	0.012(1.0)	0.10(4)	0.42(8)	1.3(12)
$\mathcal{B}(D^+ \to K^-\pi^+\pi^+)$ [%]		9.4	9.4	9.4	9.4	9.4
stat (%)		0.004(4)	0.004(4)	0.004(4)	0.004(4)	0.004(4)
syst (%)		-	-	-	-	-
$\int \frac{d\sigma}{dp_T} \mathrm{d}p_T [nb/GeV/\mathrm{c}]$		71,000	37,000	15,900	5,030	484
stat (%)		14,000(20)	3,500(9)	1,500(9)	430(8)	42(9)
syst (%)		4,300(6)	2,200(6)	1,100(7)	500(10)	63(13)

Table 13: *Differential cross section measurement result. For the uncertainties, the number bewteen parentheses is the relative uncertainty in %.*

D^0 daughters:	COT axial hits	≥ 25
	COT stereo hits	≥ 25
	SVX z hits	≥ 1
	SVX SAS hits	≥ 2
	SVX $r-\varphi$ hits	≥ 3
	p_T	≥ 2 GeV/c
	at radius R = 133 cm, $\|z\|$	≤ 155 cm
	at radius R = 10.645 cm, $\|z\|$	≤ 47.25 cm
D^0 candidate:	$m_{\pi\pi}$	$\in$ [1.7; 1.8] GeV/c^2
π_s:	η	$\in$ [-1; 1]
	COT axial hits	≥ 25
	COT stereo hits	≥ 25
	SVX z hits	≥ 1
	SVX SAS hits	≥ 2
	SVX $r-\varphi$ hits	≥ 3
	at radius R = 133 cm, $\|z\|$	≤ 155 cm
	at radius R = 10.645 cm, $\|z\|$	≤ 47.25 cm
$D^{\star+}$ candidate:	$m_{D^0\pi_s}$	$\in$ [2.009; 2.012] GeV/c^2

Table 14: *List of cuts used in the TTT hadronic sample.*

$\mu\mu$:	COT axial hits	≥ 25
	COT stereo hits	≥ 25
	SVX z hits	≥ 1
	SVX SAS hits	≥ 2
	SVX $r-\varphi$ hits	≥ 3
	p_T	≥ 1.5 GeV/c
	at radius R = 133 cm, $\|z\|$	≤ 155 cm
	at radius R = 10.645 cm, $\|z\|$	≤ 47.25 cm
J/Ψ candidate:	$m_{\mu\mu}$	$\in$ [3.073; 3.121] GeV/c^2

Table 15: *List of cuts used in the J/Ψ sample.*